Estimation of crop water use with Sentinel -1 and 2 data integration.

KYEKU PAUL.
Enschede, The Netherlands, August 2023.

Thesis submitted to the faculty of Geo-Information Science and Earth Observation of the University of Twente in partial fulfillment of the requirement for the degree of Masters of Science in Geo-information Science and Earth Observation.
Specialization: Natural Resources Management.

Supervisors:
Dr. Michael T. Marshall

Dr. Schlund Michael

THESIS ASSESSMENT BOARD:

Chair: Dr. Ir. Anton Vrieling.

External examiner: Dr. Y. Zeng.

ABSTRACT

Evapotranspiration (ET) is an important parameter that influences the availability of water for crop production. ET comprises of two processes: evaporation, which is water loss from soil and vegetation surfaces, and transpiration, which is water release through plant roots and leaf openings. Accurate and timely information about ET is essential for understanding the global water balance, which is vital for irrigation scheduling, assessing plant water requirements, and overall water resource management. However, accurate estimation of ET, especially on a larger scale, is clogged with a lot of uncertainties. The choice of data used as input for ET estimates is a key factor contributing to these uncertainties. Similarly, the partitioning of evapotranspiration into its components of evaporation and transpiration also contributes to the uncertainties of ET estimate. To address these uncertainties and enhance accurate ET estimation, this study leveraged the capabilities of both Sentinel-1 (sensitive to canopy structure and soil moisture content) and Sentinel-2 (sensitive to photosynthesis, canopy structure, and moisture contents), by integrating their indices. The analysis was performed on two different water regimes, allowing for exclusive evaluation of the performance of Sentinel- and Sentinel-2 indices. This was essential to see if there would be differences in the predictive power of the RF model. Furthermore, the most important vegetation and polarimetric indices were evaluated. The result revealed that Chlorophyll red-edge (Chlre) was the most important vegetation index given its sensitivity to chlorophyll contents in plants. The results proved that the integrated use of Sentinel-1 and Sentinel-2 improved ET estimates on both rainfed and irrigated agriculture achieving an overall R^2 =0.67. Sentinel-2 accounted for 66% of the variability in ET. While Sentinel-1 indices explained 26% variability in ET, suggesting that Sentinel-1 cannot explain variability in ET in isolation. The result of the ET estimate for rainfed agriculture using all sensors S1+S2 (rainfed) was reduced by 2%. The outcomes of irrigated agriculture, though subject to scrutiny due to the limited sample size, exhibited a 2% improvement. This improvement was expected given the substantial occurrence of evapotranspiration in irrigated agriculture found in the literature. Overall, Sentinel-2 has contributed to the total ET in this study due to its sensitivity to chlorophyll and moisture content. These parameters are related to photosynthesis, which is directly connected to ET process.

ACKNOWLEDGEMENTS

I would like to express my heartfelt gratitude to the individuals who have been instrumental in bringing this thesis to fruition. Your unwavering support, guidance, and encouragement have been a constant source of motivation throughout this transformative journey.

First and foremost, I acknowledge the boundless blessings bestowed upon me by the Almighty God . I am profoundly grateful for the guidance, strength, and opportunities provided on this journey. My heartfelt gratitude to my dedicated supervisors, Dr. Michael Marshall and Dr. Michael Schlund. Your invaluable mentorship, expertise, and willingness to invest time and effort into guiding my research have significantly shaped the outcome of this study. Your constructive critiques and well-timed guidance have been instrumental in refining the quality of this thesis.

I am also indebted to Prof. Vrieling Anton, who chaired the thesis assessment board. Your commitment to the evaluation process and the insightful feedback you provided since the proposal defense has been immensely valuable. Your constructive criticism has contributed significantly to enhancing the depth and scope of this research.

Turning to Dr. Raymond Nijmeijer, I express my heartfelt appreciation for your empathetic approach, motivating reminders to stay focused on my goals, and the sage advice you have imparted. Your encouragement during challenging times has been a guiding light.

My deep gratitude extends to my family and friends in Ghana, whose unwavering support, genuine well-wishes, and fervent prayers have sustained me throughout my academic journey. Their belief in my potential has been a constant source of strength.

I also wish to extend my heartfelt gratitude to the Government of the Netherlands for granting me the invaluable opportunity to pursue this study through their scholarship program. This generous support has played a significant role in enabling me to undertake this academic endeavor and contribute to the field of research. The scholarship not only eased financial burdens but also provided me with a platform to enhance my knowledge and skills. I am deeply appreciative of their investment in my education and the doors it has opened for personal and professional growth.

Finally, as I approach the conclusion of this thesis and stand on the precipice of earning my MSc. degree, I am overwhelmed with profound gratitude for the individuals who have accompanied me on this arduous path. Each one of you holds a special place in my heart, and I will forever cherish the connections we have forged. Your unwavering support and belief in me have been instrumental in overcoming hurdles and celebrating victories along the way.

Table of Contents

LIST OF FIGURES.

LIST OF TABLES

LIST OF ABREVIATIONS

Abbreviations	Meaning
EC	Eddy Covariance
EO	Earth Observation
ESA	European Space Agency
ET	Evapotranspiration
GEE	Google Earth Engine
GRD	Ground Range Detection
LAI	Leaf Area Index
LE	Latent Heat
MODIS	Moderate-Resolution Imaging Spectrometer
NASA	National Aeronautics Space Administration
NDVI	Normalised Difference vegetation Index
NDVIRE	Normalized Different Vegetation red-edge
NDWI	Normalized Different Water Index
NIR	Near Infra-red
PDP	Partial Dependence Plot
PI	Principal Investigators
REIP	Red-edge inflexion Point
RF	Random Forest
SAR	Synthetic-aperture radar
SAVI	Soil Adjusted Vegetation index
SR	Surface Reflectance
SWIR	Short Wave infra-red
VI	Vegetation Index
VSURF	Variable Selection Using Random Forest

1. Introduction

1.1 Background

Water is an essential resource for several applications including agricultural production. It is the foundation of sustainable development and the driver of socioeconomic growth, the production of energy and food, the maintenance of healthy ecosystems, and human existence itself (United Nations, 2015; Chen et al., 2004) Though it is a renewable resource, competition for water is expected to increase due to increased water demands for agriculture production, urbanization, and climate- driven drying (Postel, 2000; Zhen et al., 2021). Globally, agricultural practices are deteriorating biodiversity, land, water, and climate at the same time. Irrigation agriculture, for instance, accounts for 70 percent of all freshwater withdrawals globally and has been recognized as a primary source of water depletion in many regions of the world (Anderson et al., 2012; Biggs et al., 2015; Rosegrant et al., 2009). For instance, Morocco's arable lands consume 83% of its total water resources (El Hachimi et al., 2022). Similarly, the overexploitation of groundwater in six agricultural regions of India to support agricultural production is causing water shortages estimated at 100 $x10^9$ m^3 (Postel, 2000), a quantity of water that is more than the typical annual flow of the Nile River (Postel, 2000). Climate change also influences the global water budget (Wanniarachchi & Sarukkalige, 2022). In dry regions of the world, climate change accounts for the highest water loss (Wanniarachchi & Sarukkalige, 2022). Low rainfalls and high temperatures increase the evaporation of water from the soil and vegetation canopy into the atmosphere (Chapin et al., 2006). In addition, demand for water in urban areas for domestic and industrial uses has increased with the number of people living in cities. Rosegrant et al. (2009) estimated that urbanization and industrial water demands will double from 13 % to 27%, particularly in developing countries by the year 2025. Although some ecosystems may struggle to cope with water scarcity, human society possesses the capability to adapt when offered timely information regarding water scarcity (Fisher et al., 2017).

Evapotranspiration (ET) is also an important parameter that influences the availability of water for agriculture. Evapotranspiration is the process where water undergoes a phase change, converting from a liquid state to vapor, while being transported from the surface to the atmosphere (Troch et al., 1997). ET is the collective term used to describe the combined processes of evaporation and transpiration. Evaporation refers to the process of water loss from the soil and vegetation surfaces, while transpiration involves the release of water through leaf openings called stomata (Anderson et al., 2012). The energy equivalent is latent heat (LE). ET plays a crucial role in agricultural systems, serving as a regulatory mechanism for crop water demands, ensuring that the right amount of water is provided to sustain optimal growth and development (Ito et al., 2018). As a result, it is often regarded as an indicator of soil water availability and plant health (Yang et al., 2018). Yet, it is perhaps one of the most challenging hydrological flux to quantify particularly at regional to global scale (Liou & Kar, 2014). Hydrologists and agronomists have long recognized the importance of ET due to its close connections with terrestrial water use, crop photosynthesis, and plants development in agroecosystems (Biggs et al., 2015; Penuelas et al., 1993; Yang et al., 2018; K. Zhang et al., 2016). Providing accurate and real-time information on ET is essential for quantifying the global water budget which is critical for irrigation scheduling, assessing plant water requirements, and water management (Badgley et al., 2015; Biggs et al., 2015; L. Zhang et al., 2021). Also, assessments of global ET can be used to determine, for instance, how the world's food supply system may adapt to a changing climate (Biggs et al., 2015).

With the advancement in technology, field scale ET can be estimated directly using a number of techniques, including; surface renewal methods (SR), weighing Lysimeters, scintillometers, and eddy covariance (EC) etc. (Biggs et al., 2015; Yao et al., 2018a). The SR method estimate ET by measuring heat transfer between plant canopy and the atmosphere due to temperature differences which is prevalent in areas with sufficient water supply (Y. Hu et al., 2018). Hence, the SR approach is valuable for estimating ET in well-watered agricultural systems (Y. Hu et al., 2018). The weighing lysimeter on the other hand, is one of the best ways of measuring ET on small parcel of land. The instrument operates by isolating a specific volume of soil and measuring the change in mass by monitoring the amount of precipitation that an area receives and the amount lost through the soil (Seifert Schmidt et al., 2013). In addition, scintillometers are instruments that measure the atmospheric turbulence using the principle of light propagation (Perez-Priego, 2021). Scintillometers work by emitting a laser or light beam to measure the fluctuations in the received signal caused by atmospheric turbulence. To this end, the use of the aforementioned techniques are economically expensive, time-consuming, labor-intensive, susceptible to instrument failure, and they are only able to offer localized estimates of ET (Liou & Kar, 2014). The EC method measures the exchange of gases, particularly water vapor and carbon dioxide, between an ecosystem and the atmosphere over a variety of time intervals, ranging from minutes to years (Y. Hu et al., 2018). EC towers are also considered the gold standard for estimating ET due to their direct measurements, high temporal resolution, and accurate results (Fisher et al., 2008). These features make them the preferred data source for Earth scientists studying ET. Additionally, ET data from EC are easily accessible and freely available. Moorhead et al. (2019) reaffirmed the easy accessibility of EC data, reinforcing how it had predominantly been utilized for research purposes. In summary, this study employed EC method to calibrate the model due to its easy accessibility, spatial distribution and the provision of longest time series data.

Earth observation (EO) has also provides spatially explicit and continuous information for the mapping of regional and small-scale ET on the surface of the earth (Fisher et al., 2017). Here, the term "EO" refers to the collecting of images from satellite and airborne platforms (Biggs et al., 2015). It is generally accepted as the only realistic way to obtain estimates of ET at the spatiotemporal scales and accuracy levels required for many applications (Biggs et al., 2015). Sentinel, Landsat, and the Moderate-Resolution Imaging Spectrometer (MODIS) are a few of these remote sensing datasets. The information encoded in the visible, near-infrared (NIR), Short wave infrared (SWIR), microwave, and thermal infrared bands make it possible to obtain ET estimate from these datasets (Liou & Kar, 2014). SWIR region in particular is sensitive to changes in canopy and soil moisture due to its strong water absorption characteristics (Marshall et al., 2020). The chlorophyll absorption (red) is an indicator of photosynthetic activity in vegetation (Fernández-Manso et al., 2016). As a result, plants with high amount of chlorophyll tends to absorb a greater amount of red light for their energy needs through photosynthesis. The NIR range also provides insights into the structural properties of vegetation canopies . The red-edge on the other hand, represents a transitional region between Red and NIR, where vegetation reflectance changes rapidly (Mutanga et al., 2012). This region is particularly sensitive to chlorophyll content and leaf structure properties. Vegetation indices (VIs) including; Normalized Difference Vegetation Indices (NDVI), Chlorophyll red-edge (Chlre) , and Normalized Difference Water Index (NDWI), are frequently interpreted as proxies for crop productivity and health (Khan et al., 2010). NDVI for instance relies on variations in how vegetation reflect red and NIR lights. Healthy vegetation absorbs red light for photosynthesis and reflects NIR light (Debats et al., 2016). Higher NDVI values indicates active photosynthesis, revealing insights into vegetation

density, and productivity. Chlre refers to chlorophyll red-edge index, which is a measure of the amount of chlorophyll, the green pigment in plants responsible for photosynthesis (Gitelson et al., 2003). The red-edge is the wavelength between red and the near infrared band. It is characterized by a point of maximum slope called Red-Edge Inflexion Point (REIP) (Gitelson et al., 1996). The REIP describes the chlorophyl concentration in plants. A shift in the REIP towards the blue band indicate water stress in plants whiles a shift in REIP toward the red band shows a healthy vegetation (Gitelson et al., 1996) Higher Chlre values usually indicate presents of vegetation, reflecting greater potential for photosynthetic activity and overall plant health. NDWI is sensitive to changes in water content within the plant tissues, which can be indicative of plant stress or health (Khan et al., 2010). These vegetation indices are calculated from specific combinations of spectral bands, which serve as input variables for ET models (Marshall et al., 2020). That said, the use of remote sensing data have gained popularity due to several advantages it offers. One is its affordability , as remote sensing data has become more accessible and cost-effective over time (Tasumi, 2019; Yao et al., 2018b). Remote sensing provides a means to obtain data on a large scale, covering large areas, and capturing detailed geographic information that may not be easily accessible through ground-based methods (Khan et al., 2010).

Given that remote sensing does not directly measure evapotranspiration (ET), it becomes crucial to apply modeling techniques to translate remote sensing data into meaningful ET estimates. This has led to the development of various methods, as explored by K. Zhang et al. (2016), for estimating ET by utilizing remote sensing data as inputs. These methods can be classified into Direct, indirect and data-driven methods. Direct methods estimates ET from net radiation directly (Cleugh et al., 2007). Example includes, Priestley Taylor-Jet Propulsion Laboratory, and Penman-Monteith equation. Direct methods are widely used for large scale studies, because they requires few inputs (Jiménez et al., 2011). Indirect methods on the other hand, estimate ET by calculating the latent heat flux, which represents ET equivalent as the difference between net radiation (incoming minus outgoing energy) and sensible heat flux (heat exchange between surface and air) (Norman et al., 1995). Examples includes, Atmosphere-Land Exchange Inverse (ALEXI) and Surface Energy Balance (SEB). However, it should be pointed out that direct and indirect methods struggled to accurately capture the complex underlying processes of ET, particularly in areas with varying local conditions, specifically when applied in moisture-limited areas (X. Hu et al., 2021a). Data-driven method on the other hand, measure ET directly from input data using machine learning algorithms like random forest, support vector machines, and neural networks (Kumar et al., 2002). Tuning parameters and interpretation are the challenges to the application of machine learning algorithms (X. Hu et al., 2021b). Although there is no unified solution to solving this problem, Kumar et al. (2002) proposed several strategies including grid search, feature reduction, increase sample size, random search, and Bayesian optimization. Again, machine learning algorithms are able to explain complex underlying physical processes governing ET (Biggs et al., 2015). This ability is attributed to their capacity to recognize intricate patterns, interactions, and nonlinearities that may not be easily discernible through the direct and indirect methods (X. Hu et al., 2021b). Specifically, this study employed random forest algorithms, since it is the most widely used shallow learner in field of Earth observation. This is due to its ensemble learning capabilities, which can lead to more stable and accurate predictions by reducing the impact of individual trees biases (Breiman, 2001). Furthermore, random forest does not assume a specific data distribution; instead, it relies solely on the data itself (El-Baroudy et al., 2010). This characteristic makes it well-suited for capturing intricate relationships. Furthermore, random forest tends to outperform other methods in various application, as demonstrated in studies by (X. Hu et al., 2021a; Kumar et al., 2002).

However, accurate ET estimation in the scientific literature is still clogged with a lot of uncertainties. A significant part of these uncertainties is connected to both the choice of the model used and the data inputs incorporated into the ET estimation process (Badgley et al., 2015). Thus, ET estimates can be scale-up from local to regional scale by using remote sensing-based ET models calibrated with in situ data (Van Dam et al., 2006). However, these models inherently involve simplifications and assumptions that might not fully capture the complexity of real-world conditions. This disparity between model representation and actual phenomena introduces uncertainties into the ET estimation process. Equally significant for accurate and reliable ET estimation relies on the quality and suitability of inputs data. Any errors, inconsistencies, or biases within these input datasets can propagate throughout the modeling process, amplifying uncertainties in the final ET outcomes (Kingston et al., 2009). Moreover, accurately partitioning total ET into its components of evaporation and transpiration also poses challenge to ET measurement (Badgley et al., 2015). Transpiration accounts for about 57.2% of the total ET on the earth surface making it the most researched component of ET (Schlesinger & Jasechko, 2014). Soil evaporation is also important to the total ET estimate but difficult to distinguish the contribution of soil evaporation to total ET (Liou & Kar, 2014; Purdy et al., 2018). While soil moisture indicates soil evaporation, multispectral Earth observation data typically lacks the granularity required for accurate measurement of soil evaporation (Liou & Kar, 2014). This inadequacy can be attributed to the relatively coarse spatial resolution of the data, which makes it challenging to capture the finer variations in soil moisture necessary for precise soil evaporation estimation (Lowder et al., 2016).

To reduce the uncertainties and improve ET estmate, this study employed high quality data by integrating Sentinel-1 and Sentinel-2. This integration is particularly valuable due to the distinct nature of the processes driving soil evaporation and canopy transpiration, which requires different data to capture this processes. Generally, Sentinel-2 multispectral imagery which is the target variable for this analysis, offers valuable insights into land cover, vegetation health and surface characteristics, which can contribute to a comprehensive understanding of ET. Sentinel-2 includes two satellites, Sentinel-2A and Sentinel-2B, with revisit cycles of 5 days when both satellites are active (ESA, 2023). As a results it has been used for monitoring changes in vegetation and land surface (2021), monitoring irrigation events Ma et al. (2022) and to study crop water use in agriculture (Vanino et al., 2018). Moreover, Sentinel-2 provides high spatial resolution imagery, capturing details of earth surface, essential for distinguishing various land cover types, vegetation patterns and changes overtime (Xun et al., 2021). However, the limitations of optical imagery under cloud cover and during nighttime operations can hinder its comprehensive data collection for ET estimation. The Synthetic Aperture Radar (SAR) technology of Sentinel-1 transcends these limitations, delivering data regardless of weather conditions. This is made possible because, Sentinel-1 is an active remotes sensing technology that operates based on radar signals. They transmit electromagnetic pulses and receive the echoes of the backscattered signal after they interact with earth surface (Moreira et al., 2013). This capabilities ensure consistent data availability, and reducing uncertainties associated with data gaps (Harfenmeister et al., 2019). Moreover, Sentinel-1 capability to penetrate vegetation and soil provides a unique advantage in accurately estimating ET, especially in regions with intricate landscapes and variable vegetation cover (Lu et al., 2016). Though, data from both sensors are freely available, to our knowledge they have not been integrated for ET estimate on a large scale. The integration of Sentinel-2 with Sentinel-1 using data-driven method was therefore an

attempt to explore the complementary information offered by each sensor in order to reduce the uncertainties and enhance the accuracy and the reliability of ET estimate on a global scale.

1.2 Problem statement

The choice of inputs for accurate measurement of ET for effective water management has been a long-standing problem both in literature and international development agenda. The problem arises from the fact that soil moisture, which often serve as surrogate of soil evaporation, is often misrepresented (Badgley et al., 2015). Vegetation indices existing in the literature, derived from multispectral or hyperspectral data are designed to capture the photosynthetic activity of the canopy (Marshall et al., 2016). By extension they are a good proxy for crop transpiration component of total ET process. However, these indices are not capable of measuring soil evaporation particularly during the period where canopies are fully developed (Glenn et al., 2010). As a result, soil evaporation representation remains a challenge for total ET estimation in rainfed and irrigated agriculture (Purdy et al., 2018). Studies used short wave infrared broadbands, thermal infrared broadbands, and microwave to estimate soil evaporation due to their sensitivity to soil moisture (Purdy et al., 2018). However, these portions of the electromagnetic spectrum have been studied in isolation for different applications. By integrating Sentinel-1 (sensitive to canopy structure, canopy and soil moisture content) and Sentinel-2 (sensitive to canopy transpiration and soil evaporation), the goal is to enhance the representation of both soil moisture and canopy transpiration to minimize uncertainties and improve ET estimate.

1.3 Research objectives, research questions, and hypothesis.

The primary aim of this study is to assess the performance of spectral indices from Sentinel-2 and polarimetric indices from Sentinel-1 in estimating evapotranspiration over crop-lands. To achieve this objective, the study aimed to identify the most important vegetation and polarimetric indices for the estimation of total evapotranspiration. Additionally, the study aimed at assessing the relationship between the spectral indices, polarimetric indices and evapotranspiration. Moreover, the research evaluated the proportion explained by each indices by sensor under rainfed and irrigated agriculture.

The detailed Sub-objectives, research question and hypothesis are:

1. To identify the most important vegetation and polarimetric indices of evapotranspiration in croplands from Sentinel-1 and Sentinel-2.

a) What is the most important vegetation and polarimetric indices in estimation evapotranspiration?

Hypothesis: Red edge, Near Infrared narrow bands from Sentinel-2 will be the most important predictors given their sensitivity to transpiration, the largest component of evapotranspiration, while Sentinel-1 backscatter VH will be more important, but less so, given its sensitivity to soil evaporation, the second largest component.

b) What is the relationship between the spectral vegetation indices, polarimetric indices and evapotranspiration?

Hypothesis: NDVI, and Chlre would demonstrate a significant correlation with Evapotranspiration given their sensitivity to crop transpiration, whiles VH backscatter will have a significant relationship with evapotranspiration, but less so given its sensitivity to soil evapotranspiration.

2. To assess the relative proportion of total evapotranspiration explained by spectral vegetation and polarimetric indices.

a) What is the relative proportion of total evapotranspiration explained by spectral vegetation indices and polarimetric indices?

Hypothesis: The proportion of total evapotranspiration explained by spectral vegetation indices would be 10% as crop progress over the growing season.

3. To assess the relative proportion of evapotranspiration explained by spectral vegetation and Polarimetric indices on rainfed and irrigated agriculture.

a) What proportion of total evapotranspiration is explained by spectral vegetation and polarimetric indices on rainfed and irrigated agriculture?

b) What proportion of total evapotranspiration is explained by spectral vegetation and polarimetric metric on irrigated agriculture?

c) Do vegetation and polarimetric indices improve the evapotranspiration estimation on rainfed and irrigated agriculture?

2.0 Data and Methods

The following sections summarize the workflow in the integration of Sentinel-1 and Sentinel-2 for total ET estimation. The main steps that were taken are presented in **fig.1** below. The first step was to acquire Sentinel-1, Sentinel-2 data, Moderate Resolution Imaging Spectrometer data (MODIS) and Eddy covariance data (EC). Both Sentinel-1 and Sentinel-2 data were acquired from Google Earth Engine (GEE), MODIS from AppEARS whiles EC data were acquired from 15 flux tower stations specifically from Ameriflux and Euroflux. Sentinel-2's reflectance data were used to derive vegetation indices, while Sentinel-1 backscatter data were used to derive polarimetric indices. Variables Selection using random forest (VSURF) package in R was used to eliminate irrelevant and redundant variables. The important variables selected by VSURF were used to build random forest (RF) model. The RF model was subsequently used to predict ET for rainfed, irrigated ET, transpiration and soil evaporation. The purpose was to determine the proportion of ET that could be attributed to spectral vegetation and polarimetric indices. Finally, the model was subjected to accuracy *assessment to ascertain the goodness of fit of the proposed RF model.*

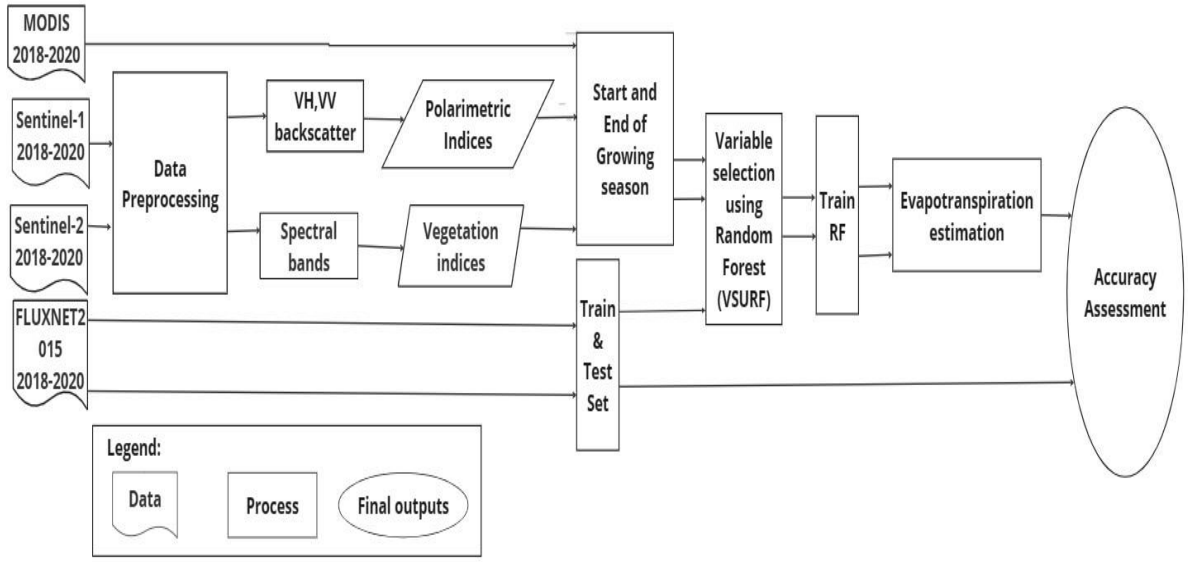

Figure 1. Technical workflow.

2.1.1 Data acquisition and processing

2.1.2 Eddy covariance and micrometeorological measurements

Ground-scale ET data used as reference data were acquired from 15 eddy covariance flux towers across major agroecological zones. The 15 selected eddy covariance flux tower sites were specifically chosen due to their availability of continuous data spanning a period of three years or longer. This was necessary for the reduction of data gaps which could arise from due sensor malfunctions, and weather conditions (Falge et al., 2001). Moreover, 3 years of continuous data was necessary to facilitate the validation of the model under a wide range of conditions, such as different seasons, vegetation growth, and variations in soil moisture (Fisher et al., 2008). All 15 selected sites are croplands consisted of wheat (4 sites), soybean (2 sites), rice (1 site), and corn (8 sites). Generally, these crops were chosen because they

represent major staple food crops with significant global agricultural importance (Oerke & Dehne, 2004). From the 15 selected sites, 11 sites were rainfed, 4 sites were irrigated. 10 sites were acquired from AmeriFlux available at: (ameriflux.lbl.gov), and 5 from EuroFlux available at: (https://fluxnet.org/data/fluxnet2015-dataset/). Micro-meteorological variables from this sites included, latent heat flux (LE, W m^{-2}), sensible heat (H Wm^{-2}), relative humidity and ground heat flux (G m^{-2}). The LE variable acquired from AmeriFlux were recorded at a daily time step and gap-filled using the marginal distribution sampling approach and linear interpolation with locally weighted regression (Pastorello et al., 2020). However, LE variable acquired from EuroFlux: BE-Lon, CH-Oe2, FR-Gri, DE-Kli, and DE-Rus, were available and recorded at a half-hour time step. Half-hourly LE data (LE W m^{-2}) was converted into daily averages by multiplying the half-hourly LE by the number of hours in a day, and smoothed using a 5-day exponential filter. Subsequently, the LE data from the 15 sites were converted from Wm^{-2} to MJ $m^{-2}d^{-1}$. Table 1. and Fig. 2 show the distribution and location of each sites.

Table 1. EC flux Stations and their information.

Site	Site Name	Lon	Lat	Crop Grown	Mean annual Temp ^{0}c	Annual precipitation (mm)	System
BE-Lon	Lonzee	4.7461	50.5516	Corn	10	800	Rainfed
CA-ER1	Elora Research Station	-80.4123	43.6405	Corn	6.7	946	Rainfed
CH-OE2	Oensingen2 crop	7.7343	47.2863	Wheat	9.8	1155	Rainfed
US-ROI	Rosemount-G12	1.9497	44.7143	Soybeans	6.4	879	Rainfed
DE-Kli	Klingenberg	13.5267	50.8937	Corn/Wheat	7.6	842	Rainfed
DE-Rus	Selhausen Juelich	6.4471	50.8659	Wheat	10	700	Irrigated
FR-Gri	Grignon	1.9497	48.8447	Wheat	12	650	Rainfed
US-Twt	Twichell Island	-121.653	38.1087	Rice	15.6	421	Irrigated
US-ARM	Arm Southern Great Plainds site-Lamont	-97.4887	36.6068	Corn	14.8	843	Rainfed
US-Bi2	Bouldin Island corn	-121.535	38.1091	Corn	16	338	Rainfed
US-CF1	CAF-LTAR Cook East	-117.082	46.7815	Corn	9	550	Rainfed

US-NE1	Mead-irrigated maize site	41.164	-96.477	Corn	10.1	790	Irrigated
US-Ro5	Rosemount I18_South	-93.0578	44.6946	Corn	6.4	879	Rainfed
US-Ro6	Rosemount L18_North	-93.0576	44.691	Soybeans	6.4	879	Rainfed
US-CS3	Central Sands Irrigated Agricultural Field	-89.5727	44.1394	Corn	7	830	Irrigated

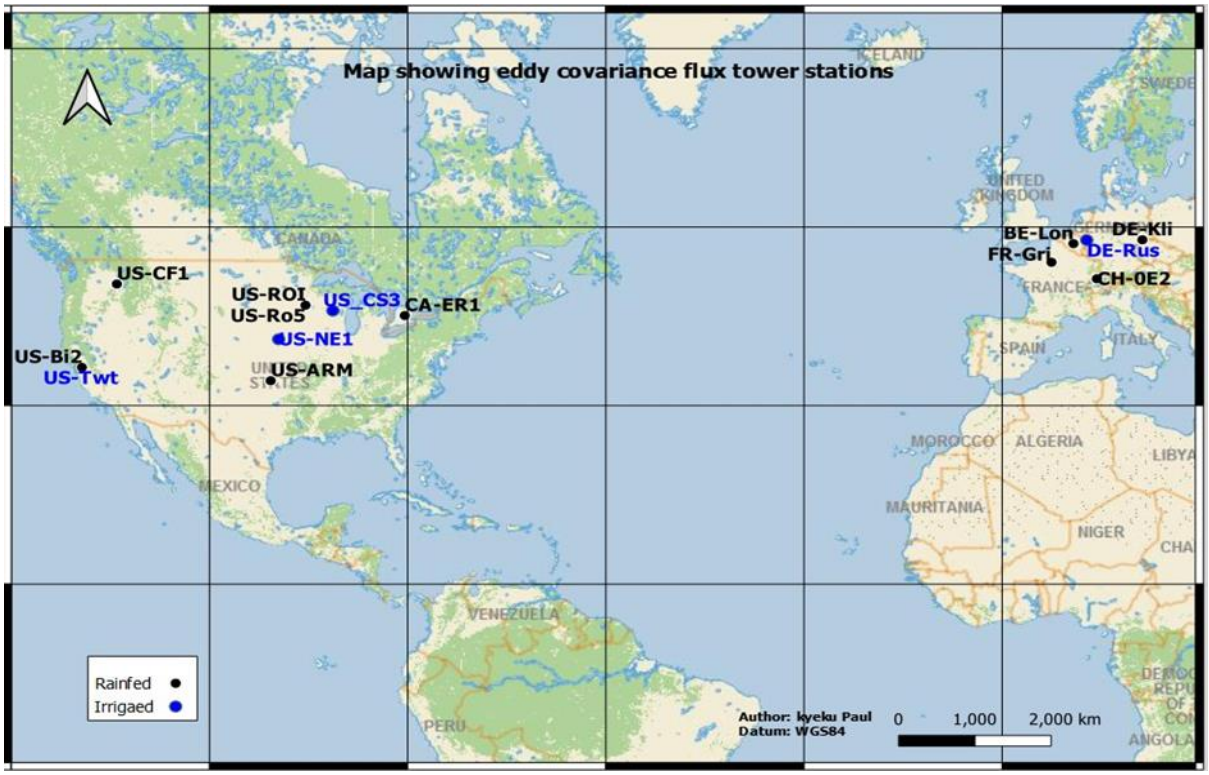

Figure 2. Map of Flux towers distribution

2.1.3 Satellite data used and acquisition.

2.1.4 Satellite data used

Three datasets derived from satellite remote sensing were used for this study. Sentinel-1, Sentinel-2, and Moderate Distance Image Spectrometer (16-day composites). The Sentinel-2 level 2A bottom-of-the-atmosphere data were accessed through the Google Earth Engine platform available at: (https://code.earthengine.google.com/). The Sentinel-2 level 2A data in GEE has been pre-processed for atmospheric and topographic effects (Praticò et al., 2021). For this analysis, the preprocessing of the Sentinel-2 data in GEE was mainly filtering and selecting images from the Copernicus Sentinel-2 Surface Reflectance (S2-SR) image collections. The filtering included selecting images within the specific date range for which there were EC data (2018-2020). Additionally, the "maskS2clouds" function was utilized to

apply a cloud mask to the Sentinel-2 images, effectively removing cloud-covered pixels from the analysis. Only pixels with a cloud coverage under 10% were retained for the analysis. The table 2 below shows the specification of Sentinel-2 data used in this study.

Table 2. Sentinel-2 specifications used in this study.

Satellite	Sentinel-2
Spatial Resolution & Bands	10m(B2,B3,B4,B8), 20m (B5,B6,B7,B8A,B11,B12)
Revisit Cycle	5 days (Sentinel-2A and Sentienl-2B)
Swath	290 km
Date Range	2018-2020
Data source	Google earth engine (http://earthengine.google.org).

Sentinel-1A and Sentinel-1B under the Copernicus program by the European Space Agency were used for this analysis. The Sentinel-1 products that are readily available include Level-1 data, which come in two formats: Single Look Complex (SLC) and Ground Range Detected (GRD) (Reiche, 2015). Similarly, Sentinel-1 offers data in three acquisition modes: Interferometric Wide (IW) swath, Extra-Wide swath and Stripmap (SM). Ground Range Detected (GRD) acquired in the Interferometric Wide mode were used for this study. The GRD product available on GEE were radiometrically calibrated, multi-looked, which improves the signal-to-noise ratio and enhances the quality of the imagery (Devries et al., 2020). The IW mode is the main operational mode for Sentinel-1 which offers information on land surfaces and is commonly used for large-scale mapping (Torres et al., 2012). The IW mode of Sentinel-1 C-band is provided in dual-polarizations combinations: vertical transmit and vertical receive (VV) and vertical transmit and horizontal receive (VH). Their pixel spacing is 10 m. Owing to its 6 day revisit cycle, Schlund & Erasmi (2020a), used it to study phenology of wheat. Other applications includes, crop mapping (Xun et al., 2021), estimating of soil moisture (Liu et al., 2021), and quantitative estimation of biophysical variables in vegetation (Frampton et al., 2013). A summary information of Sentinel-1 is presented in table 2.

Table 3. Overview of Sentinel-1 data used in this analysis.

Data Characteristics	Descriptions
Satellite	Sentinel-1A & Sentienl-1 B
Revisit Cycle	6- days for both Satellites
Polarization	VH & VV Polarization
Pixel Spacing	10m x 10m

MODIS data were not directly used as input for the ET model but were used to define the start of season (SOS) and end of the season (EOS) for crops grown on the 15 sites used in this study. This choice was influenced by the continuous data provided by MODIS, which enabled the tracking of daily and gradual vegetation changes throughout the growing season which is not possible using Sentinel-1 and Sentinel-2 indices due to their revisit cycles (Sun et al., 2012). The MODIS 16-day NDVI product was acquired from AppEARS available at:

appeears.earthdatacloud.nasa.gov. A Savitzky-Golay filter as recommended by Chen et al.(2004), was applied to the MODIS 16-day NDVI product. This filter was used because it reduces noise, fill gaps and smooth any remaining data inconsistencies (Chen et al., 2004).

2.1.5 Sentinel-1 data and Sentinel-2 data preprocessing

Sentinel-2 reflectance and Sentinel-1 backscatter values were acquired from GEE data catalog, covering the period between 2018 to 2020. The backscatter and reflectance values were extracted around the crop fields where the eddy covariance fluxes were stationed. To extract the Sentinel values, point features were generated based on the longitude and latitude coordinates of each flux tower site in GEE. A rectangular buffer area of size 60m x 60m was generated around the locations on the fields where the flux towers were stationed. The decision to adopt a buffer size of 60m x 60m was based on Sentinel-2, the target resolution of 20m for the analysis. This selection aligns with the suggestions by Congalton (2001), who proposed a buffer size three times the target resolution of any given studies. The rectangular shape buffer was due to the shape of the fields on which the flux towers were located. These buffer areas served as the sampling zone for extracting the Sentinel-1 and Sentinel-2 values. The values for Sentienl-1 and Sentinel-2 were extracted by taking the average pixel values within the 60 x 60 buffer. The average values obtained were used as the representative values for that flux tower. It is important to note that, GEE platform automatically performs the preprocessing steps and extract the Sentinel-1 backscatter and Sentinel-2 reflectance values for each pixel in the buffer area.

2.1.6 Vegetation and Polarimetric metrices.

The VV and VH polarization from Sentinel-1 and Sentinel-2 bands, were used to derived polarimetric and vegetation indices (VI) to estimate ET. The Vegetation indices including Sentinel-2 bands shown in table 2 were used as inputs for ET estimate. VIs were incorporated because, they minimize the impact of soil background, atmospheric constituents and other sources of noise that can impede the ET estimate (Vreugdenhil et al., 2018). The Normalize Difference Vegetation Index (NDVI) for instance, is suitable for assessing crop health and development (Tucker, 1979). It is also sensitive to chlorophyl contents (red) and cell structure of canopies (NIR) (Becker & Choudhury, 1988). These parameters are directly related to the process of photosynthesis in plants and, in turn, impact the transpiration of water from plants into the atmosphere, which ultimately affects the overall ET process. The red-edge1 Normalized difference vegetation indices ($NDVI_{RE1}$), red-edge2 Normalized difference vegetation index ($NDVI_{RE2}$), and red-edge3 Normalized difference vegetation indices ($NDVI_{RE3}$) calculated with (red-edge1 band 5, red-edge2 band 6 and red-edge3 band 7) and the red-edge4 band8A are known for their sensitivity to vegetation chlorophyll and water contents. The red-edge captures light wavelengths that are slightly longer than those captured by the traditional red band, but shorter than those captured by the near-infrared band. This unique position allows it to detect specific spectral signatures related to vegetation characteristics that are not as prominent in the red or near-infrared bands (Fernández-Manso et al., 2016). Chlorophyll red-edge index (CHlre) on the other hand, is known for its ability to discriminate between chlorophyll pigment (a + b) and reduced intra-species reflectance variation (Gitelson et al., 2003). This index was necessary for this analysis due to its valuable information it provides about the presence and health of chlorophyll in vegetation. The Normalized Difference Water Index (NDWI) is used to assess the amount of liquid contents in plants (Hamrell, 2014). Since the analysis was performed on different water regimes, utilizing NDWI would help detect shifts in water availability within both plant canopy and

soil, a valuable information about the broader water dynamics, enhancing the precision of ET predictions. The Soil Adjustment Vegetation Index (SAVI) is often regarded as a revised version of NDVI because it has a soil adjustment parameter that compensates for the sensitivity of NDVI to wet and dry soil background (Alam et al., 1996). By incorporating soil adjustments, SAVI provides a more accurate representation of vegetation density and health, thus enhancing the reliability of ET estimates.

The Sentinel-1 indices, (VV/VH), VV-VH, and VV+VH used for this analysis were also calculated using the backscatter coefficients of VV and VH polarization. The backscatter measurements were initially represented in decibel (dB) in Google Earth Engine (GEE), after which a transformation to a linear scale was carried out. This was important because, performing arithmetic operations directly on values in decibels can lead to inaccurate results or misinterpretations. For instance, in the decibel scale, adding or subtracting values does not correspond to simple arithmetic addition or subtraction (Becker & Choudhury, 1988). Converting to linear scale allows you to perform these operations correctly. The conversion from dB scale to linear scale was conducted using the formulae below.

$$\textbf{Linear scale} = 10^{(dB/10)}$$

Where dB is the backscatter values in decibel. The Sentinel-1variables in the linear scale were used to train RF model, allowing for the selection of the most important variable for ET prediction. However, it was converted into dB scale for visualization of the relationship between ET and Sentinel-1 indices. Table 4 and Table 5 provide a summary of the vegetation and polarimetric indices used in this analysis.

Table 4. Sentinel-2 Vegetation indices

Multispectral broadband indices	**Abbreviations**	**Equations**	**Source**
Normalized Difference vegetation index	NDVI	$\frac{B8 - B4}{B8 + B4}$	(Tucker, 1979)
Narrow band red-edge1 Normalized difference vegetation indices	$NDVI_{RE1}$	$\frac{B8A - B5}{B8A + B5}$	(Fernández-Manso et al., 2016)
Narrow band red-edge2 Normalized difference vegetation indices	$NDVI_{RE2}$	$\frac{B8A - B6}{B8A + B6}$	(Fernández-Manso et al., 2016)
Narrow band red-edge3 Normalized difference vegetation indices	$NDVI_{RE3}$	$\frac{B8A - B7}{B8A + B7}$	(Fernández-Manso et al., 2016)
Chlorophyll red-edge index	CHlre	$\frac{B7}{B5} - 1$	(Gitelson et al., 2003)
Normalize Difference water Index.	NDWI	$\frac{B8 - B12}{B8 + B12}$	(Hamrell, 2014)
Soil Adjustment Vegetation Index.	SAVI	$\frac{(B8 - B4)(1 + XSAVI)}{(b8 + b4) + XSAVI}$	(Alam et al., 1996)

Table 5. Sentinel-1 Polarimetric indices.

Polarimetric metrics	Purpose	Source
VV	Sensitive to crop growth and development.	(Nasirzadehdizaji et al., 2019)
VH	Sensitive to leaf area and crop biomass	(Harfenmeister et al., 2019)
VV-VH	Less responsive to changes in soil moisture during crop growths and development	(Gorrab et al., 2021)
VV+VH	Sensitive to crop height through the planting season	(Gorrab et al., 2021)
VV/VH	Sensitive to both vegetation structure and moisture.	(Vreugdenhil et al., 2018)

2.1.7 defining the start of season and end of season.

The NDVI-defined phenology from MODIS 16-day composites acquired on the fields where the 15 flux tower were located were used to define the start of season and end of season. This was crucial since these periods coincide with crop presence in the fields. For each of the 15 sites under study, the SOS and EOS season were determined using the delayed moving average method which is adapted from the auto regression moving average model (Reed et al., 1994). The SOS was defined as the point where NDVI temporal profile (blue line) crossed the smooth profile (moving average) curve (red dash line) in the upward direction. The EOS on the other hand, was defined as the point where the NDVI temporal profile crossed the smooth curve in downwards direction. The smooth profile curve representing the moving average was defined by window size 7 days. Using 7-days was motivated by the consideration that this timeframe is sufficient to detect significant changes associated with the onset and harvest of crop growth in the field. The start and end of the season information was then used to omit Sentinel-2 spectral values and Sentinel-1 backscatter outside the growing season from the analysis. Subsequently, date matching was carried out on Sentinel-2 and Sentinel-1 extracted values to compensate for their different temporal resolutions. The study applied 7 days time lag to align observations between both sensors. This approach recognize that although plants begin responding to changes immediately, it might take a few days to become noticeable. 7 days time lag can help capture the combined effects of plants responses to changing conditions over multiple days (SIMS & PEARCY, 1994). Furthermore, the ET values from both sensors were averaged over that period. In total, a master file containing 22 variables which consisted of 5 Sentinel-1 variables and 17 Sentinel-2 variables and 464 observations were used for ET estimate. Fig. 3 below presents a delayed moving average method for US-Ro6 site.

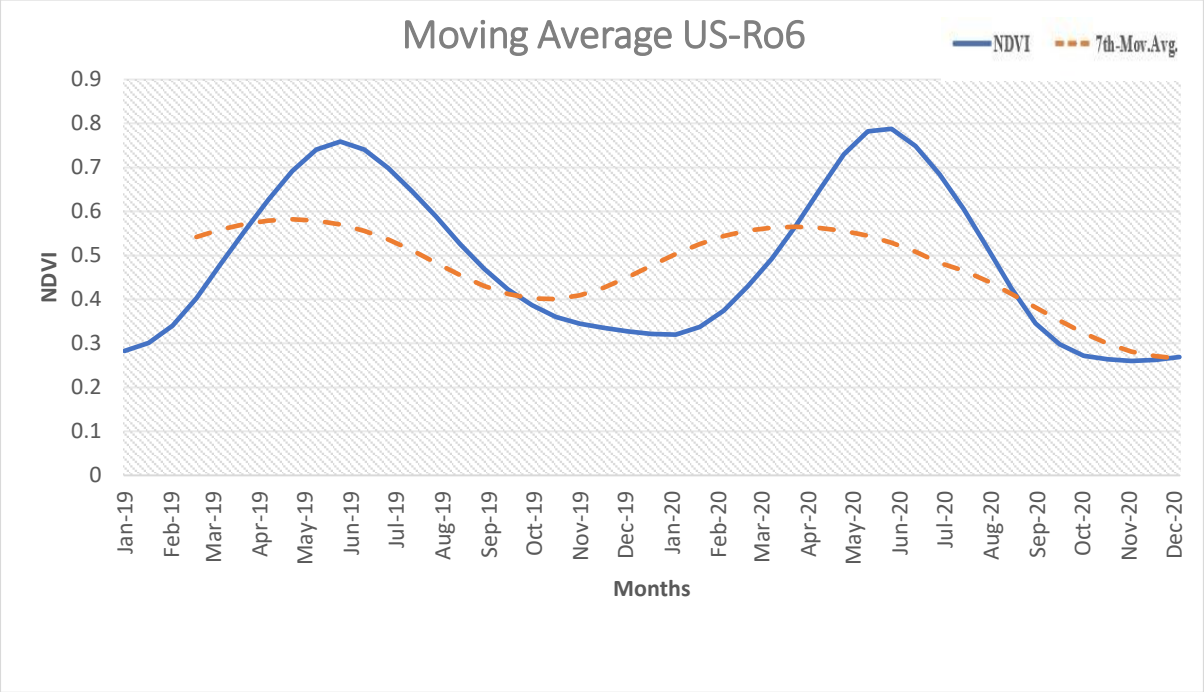

Figure 3. Start of season and end of season.

2.1.8 Training Random forest and Variable Selection using Random Forest (VSURF)

Variable Selection was conducted to assess most important variables and enhance accurate ET estimates for this analysis. As reported by Maya Gopal & Bhargavi (2019), the goal of variable selection is to remove non-informative variables from a data in order to enhance the model performance, reduce the complexities of the model and making it easier to interpret. To achieve the aim of assessing key variables and improving ET estimation accuracy in this analysis, we utilized Variable Selection using Random Forest (VSURF). This was due to RF ability to provide a measure of feature importance and indicating which features are most relevant for making prediction (Touw et al., 2013). In addition, RF produces models with more predictive power and lower error than other techniques and does not easily over-fit (Belgiu & Dra, 2016).

That said, the dataset created in chapter 2.1.7 with 464 samples was split into training and test set. The splitting was based on temporal criteria which was performed independently for each site. Since each site contained three years of data, one year was used for testing, whiles two years were used for training. This aligns with Congalton (2001) who stated that, it can help break down spatial autocorrelation by introducing temporal independence and capturing the natural variability present across different years. The training set consisted of 303 observations and the validation set consist of 161 observations. The training set consisting of 303 observation and 22 variables were used to train random forest for feature selection. It associated package in R called "variable selection using random forest "(VSURF) was used for the variables selection. The version v.1.2.0 VSURF used is available in the Comprehensive R Archives Network (CRAN) at (https://cran.r-project.org/package=VSURF.)

The Variable selection using VSURF is a three step process. The first phase referred to as the preliminary elimination (thresholding), removes irrelevant variables after several iterations. In this study the number of iteration was set to 20 to reduce the computational time. Variable

were ranked according to their mean importance score, beginning with variables with the highest importance scores. Next a decision tree was built using the standard deviation of the variable importance scores, and a minimum threshold was set (Genuer et al., 2015). Any variable with an important score less than the threshold was remove from further analysis. For this analysis after 20 iterations 12 variables were retained.

In the second phase referred to us the interpretation phase, eliminate redundant variables but some redundancies still remain. As a result, a new sets of RFs were built, starting with the 12 with the variables identified in the thresholding phase. Then, additional RFs were built, each using a different combination of variables from the selected subset in a stepwise manner until all variables selected in the thresholding phase were included. During the process, a new threshold was set by calculating the minimum mean out-of-bag (OOB) error of the random forest and their standard deviation (Genuer et al., 2015). The RF model with the least number variables, but still achieving a mean OOB error less than the "min error" was selected. The variables used in the chosen RF models were considered as the final selected variables in this phase. 12 variables were selected in this phase.

The final phase representing the predictive phase, a stepwise selection of variables was performed, beginning with the variables selected in the first phase. A variables was selected if it inclusion to the RF model would results in a significant decrease in OOB error, exceeding the threshold referred to as the "mean jump value". The mean jump value was determined using the unselected variables from the interpretation phase. It represents the average difference in OOB error between a model and the subsequent model when variables are added one by one in a stepwise manner. 6 variables were selected in the last phase and were used to train RF. parameters as recommended by Belgiu & Drăgu (2016), were defined which are the number of trees *Ntree* and number of variables *Mtry*. For this analysis the parameter *Ntree* was set to 500 as noted by Lawrence et al.(2006) that, errors stabilize before reaching this number of trees in the random forest model. To reinforce this point, Belgiu & Drăgu (2016) proposed that, the default value of 500 for *Ntree* is an acceptable value when using RF on remotely sensed data. In the case of *Mtry*, the number of variable to be considered in each split of the RF model was determined by dividing the total number of variables selected through the VSURF process by 3 (Mutanga et al., 2012).

2.1.9 Partial Dependence Plots (PDP)

Identifying the most significant variables is vital for simplifying data analysis, cutting down on computational demands, and enhances processing speed. However, as highlighted by Sheikholeslami and Dowling (2019), the most important variables might not offer a comprehensive information about the relationship between input parameters and the predicted outcomes, as well as the manner in which changes in input variables influence predictions.
Nonetheless, PDPs proved to be a valuable in analyzing input variables on predicted outcome and how changes in input variables influences predicted results. Friedman (2001) underscore this assertion, stating that PDPs explains the marginal effects that individual or pairs of variables have on the predicted outcome of a machine learning model. Moreover, PDPs serve as a form of validation by confirming whether the observed relationships align with what we expect based on our knowledge of the subject matter. Figures 11,12,13,14,15, and 16 show the PDPs for the variables selected for the first scenario.

2.2.0 Accuracy assessment.

To evaluate the performance of the final model, four statistical parameters were used. They are, coefficient of determination denoted as R^2, the root mean square (RMSE), Relative root mean square error rRMSE and Bias. The R^2 quantifies the proportion of variance in the predicted variable that can be explained by the model. It was calculated by dividing the sum of square residuals (SSR) by the total sum of squares (SST) and the result subtracted from 1. It ranges from 0 to 1, with values close to 1 indicates a better fit of the model to the data . The second parameter, root mean square error (RMSE), is a commonly used metric to measure the overall error of a model. It is derived by taking the square root of the average of the squared differences between predicted and observed values. RMSE provides insight into how closely the model's predictions match the actual observation, giving a sense of the accuracy of the model's performance. A lower RMSE indicates a better alignment between predictions and observed values. The rRMSE error is the square root of the average of squared difference between the predicted and the observed value. Bias, reflects the average difference between predicted and observed values across the entire dataset. It was calculated by summing up all the differences and dividing by the total number of data points. A smaller Bias value indicates that the model's predictions are, on average, closer to the true values.

2.2.1 Proportion of ET explain by vegetation and polarimetric indices on Rainfed and Irrigated agriculture.

To assess the proportion of ET explained by VI and polarimetric indices the method referred to as Ablation was conducted. An Ablation involves systematically removing factors, in this case variables such as vegetation and polarimetric indices, from the analysis to observe how their absence impact the explained proportion of ET (Sheikholeslami & Dowling, 2019). To assess the proportion explained by Sentinel-1 and Sentinel-2 indices, 9 different scenarios were conducted under two water regimes. In the first, second and third scenarios, the analysis predicted overall ET for all crops in both rainfed and irrigated agriculture using both Sentinel-1 and Sentinel-2 indices. Subsequently, the study predicted ET again with all crops under both water regimes using Sentinel-1 and Sentinel-2 separately. The analysis above was performed exclusively for crops under rainfed and again irrigated agriculture. The goal was to examine possible differences in outcomes among various water regimes. The table below illustrates the scenarios under for both water regimes.

Table 6. List of scenarios.

Scenarios	Crop Types	Sensor Used
1	All Crops	All Sensors
2		Sentinel-2 only
3		Sentinel-1 Only
4	Rainfed	All Sensors
5		Sentinel-2 only
6		Sentinel-1 Only
7	Irrigated	All Sensors
8		Sentinel-2 Only
9		Sentinel-1 Only

3.0 Results.

The boxplots in Figures 4 and 5 are representation of the variability of ET over rainfed and irrigated agriculture and the four crops used in this analysis. In figure 4 it can be observed that ET appears to be higher and varies more in irrigated agriculture. Usually, ET for irrigated crops are higher but with less variation in the distribution pattern. This could be due to the number of sample size for irrigated agriculture (78 samples). It could also relates to the different crop types, since different crops have varying water requirements and responses to irrigation. As illustrated in figure 5, wheat has a lower variability in ET compared to corn, soybean and rice. In rainfed agriculture with 386 samples, ET variability is lower compared to irrigated agriculture. This is due to rainfed systems relying on natural rainfall, resulting in reduced water availability and subsequently lower ET, while irrigated systems have controlled water supply leading to higher ET. Hadadi et al (2022) further elaborated on this stating that, ET is higher for wet surface than dry surface soils due to the contribution of soil evaporation. Thus, in irrigated agriculture, the balance between soil evaporation and transpiration is such that, a reduction in soil evaporation is compensated by increased transpiration, keeping total evaporation relatively stable. This mechanism contributes to higher ET in irrigated areas. In rainfed settings, water scarcity limits this compensation, leading to comparatively lower ET.

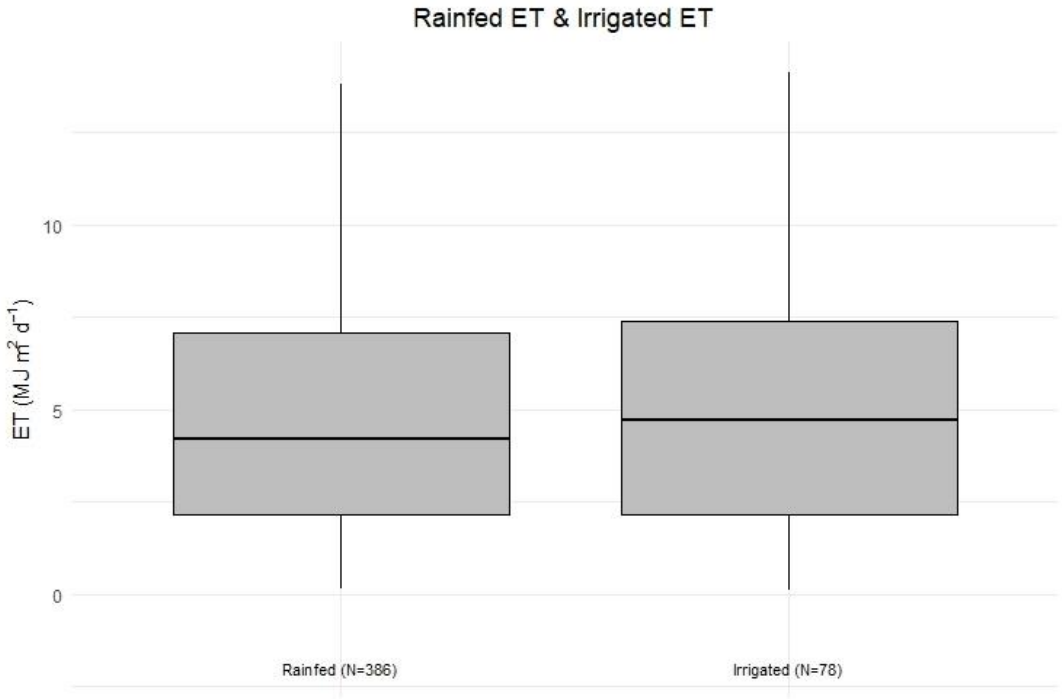

Figure 4: Boxplots for Rainfed and Irrigated ET.

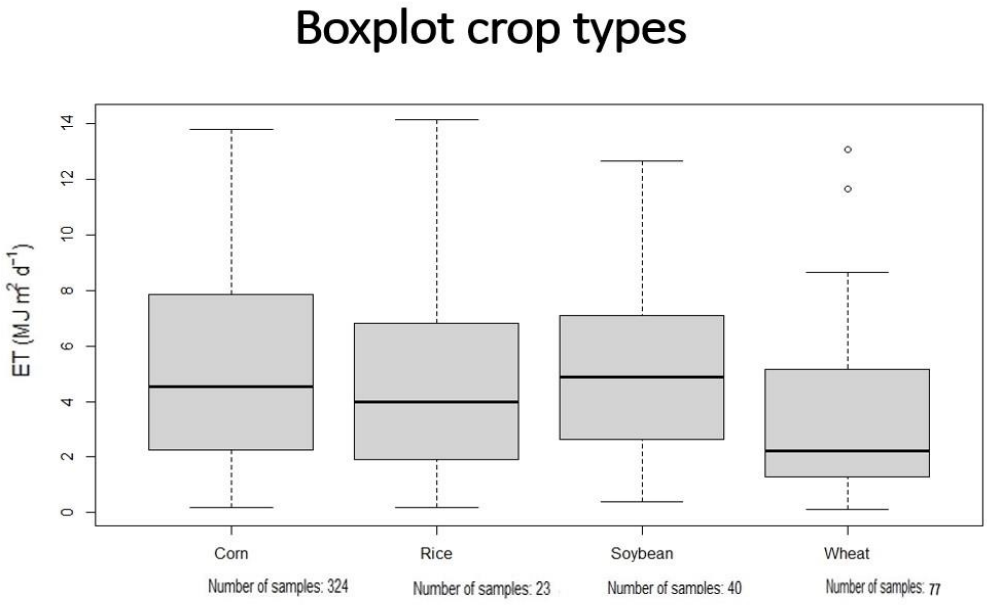

Figure 5: Boxplot of ET for different crop types.

2.1 Variable selection using Random Forest for first scenario.

Figures 6 to 9 presents the variables selection process conducted with VSURF. Figure 6 and figure 7 represent the threshold phase. The figure 6 demonstrates how variables are ranked according to their mean variable importance. Clearly variable more than 5 seems to be noisy but variables less than 5 are seen as significantly important. In figure 7 variables are eliminated
in order of importance. Based on the ranking, a plot of these standard deviations is generated, and a threshold value for VI is estimated based on this plot. A threshold as shown by doted red lines serves as a cutoff point for variable selection. Only variables with an average VI exceeding this this threshold are retained. 22 variables were retained at the threshold phase. The least OOB error was attained when using 15 variables as seen in figure 8. From the 15 variables in the interpretation phase, only 6 variables were kept after the prediction phase. Figure 9 represents the prediction phase, showing the number of variables retain.

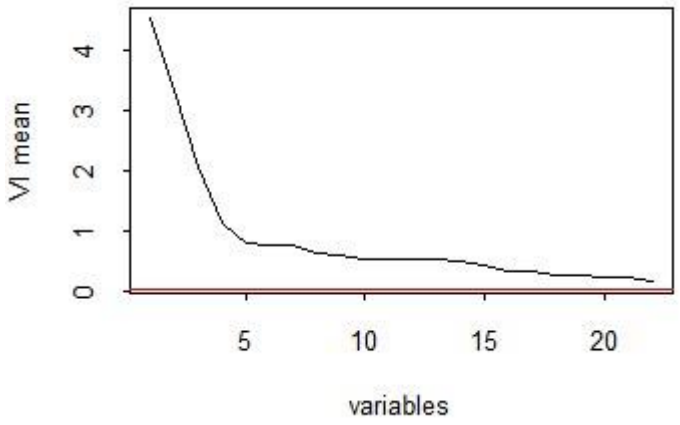

Figure 6. Variable ranking in the thresholding step.

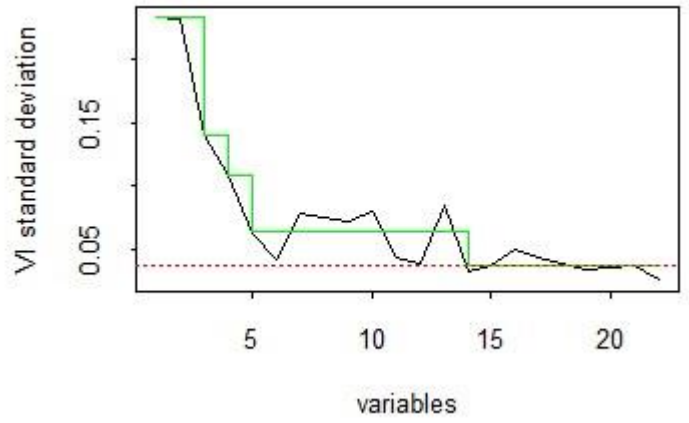

Figure 7. A step-by-step stepwise regression for variable elimination.

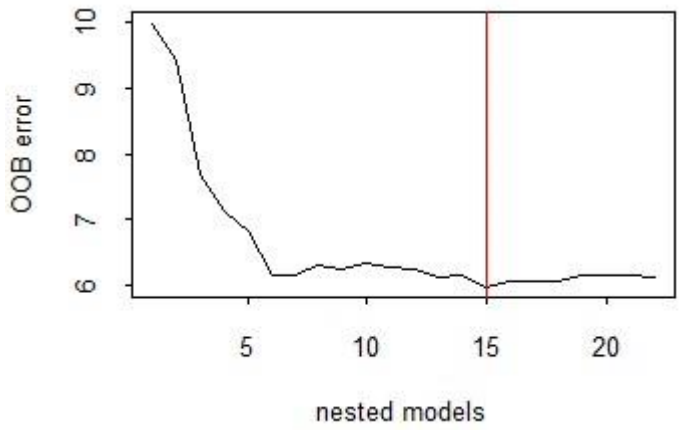

Figure 8. Nested RF Model for Model's definition with the lower OOB.

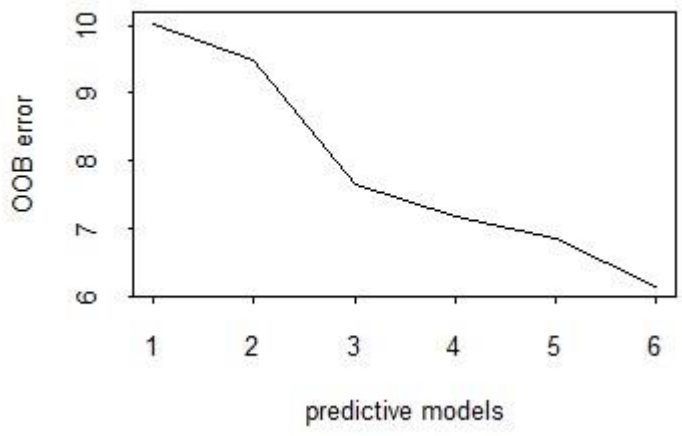

Figure 9. Predictive model based on OOB error.

2.2 Variable importance for the first scenario.

This study's primary objective was to assess the most important vegetation and polarimetric indices. As shown in figure 10, a total of 6 variables were selected namely: Chlre, Band 12 Short-Wave Infra-red, (B12_SWIR2), NDVIRE1, SAVI , VH, and NDVI. The variables importance graph demonstrates that Chlre is the most important variable with a percentage increase in mean square of error of 27.18. This implies that excluding Chlre from the model results in an approximately 27.18% rise in the error. Similarly, removing B12-SWIR leads to a 23.51% increase in the RF model's error. Among the six variables, NDVI has the least impact, causing a reduction of 15.85% in the model's error.

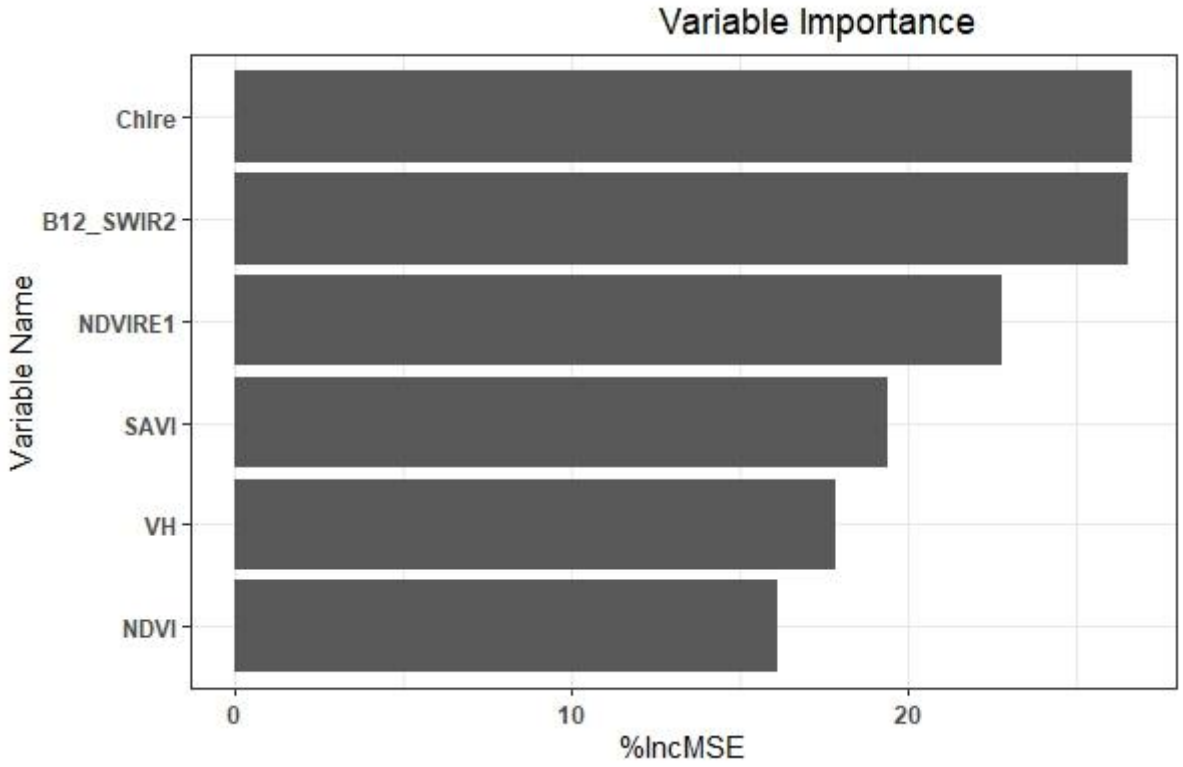

Figure 10. Variables according to their importance using increase %IncMSE

2.3 Partial Dependence Plots for first scenario.

The Partial Dependence Plots below provide a visual and intuitive way to explore the relationship between individual variables and model predictions, contributing to the interpretability of the RF models. These PDPs are specific to the first scenario, where the analysis was performed on all crops and all sensors. The PDPs are arranged in order of importance. Observing from figure 11, Chlre increases linearly with ET until around 3, after which it plateau. Meaning ET remained the same regardless of how much Chlre increases.
However, the PDP for B12-SWIR in figure 12, keep increasing with ET. This implies that ET never stops once B12-SWIR continue to increase. In contrast, the PDP for NDVIRE1 illustrates that, the relationship between ET and NDVIRE1 starts around 0.2 but ET begins to

decrease when NDVIRE1 reaches a value of approximately 0.75. The PDP for SAVI as illustrated in figure 13, also increases with ET until 0.3, but begins to increase slowly when SAVI reaches a value approximately 0.35. In figure 15, ET begins to increase when VH backscatter reaches -20. Furthermore, the relationship between ET continues to increase with increase in VH backscatter. Finally, the PDP for NDVI revealed that, ET reaches 4.92 even when NDVI was 0.0. But ET saturates when NDVI was around 0.48, but decreased to 0.5 when NDVI was approximately 0.58.

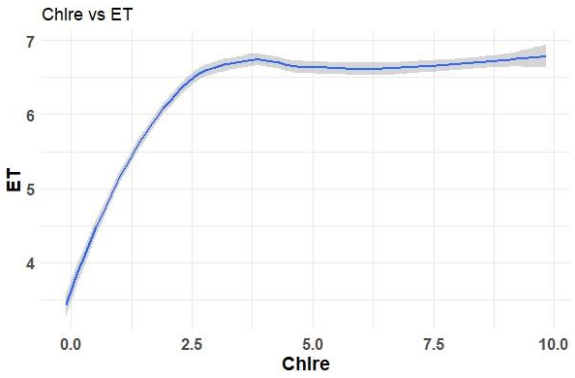

Figure 11. Partial Dependence Plot for Chlre and ET.

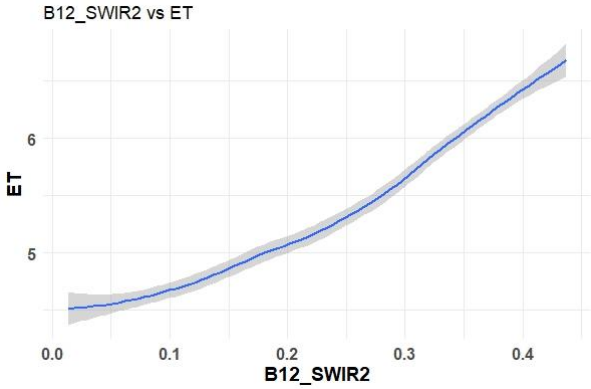

Figure 12. Partial Dependence Plot for B12_SWIR2 and ET.

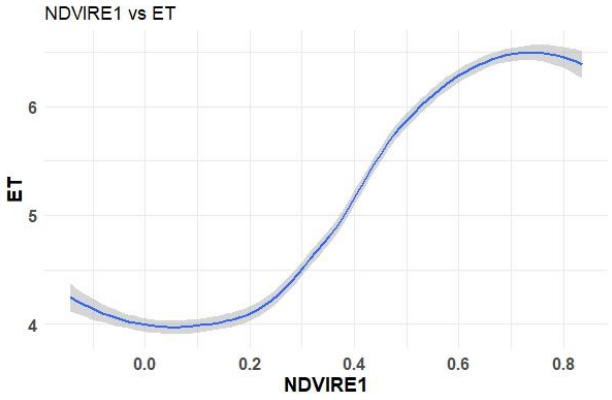

Figure 13. Partial Dependence Plot for NDVIRE1 and ET.

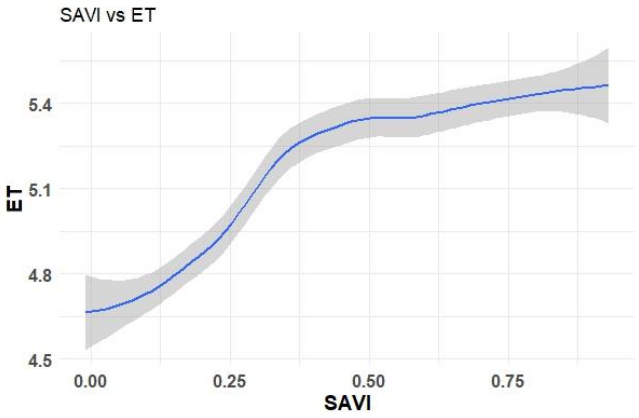

Figure 14. Partial Dependence Plot for SAVI and ET.

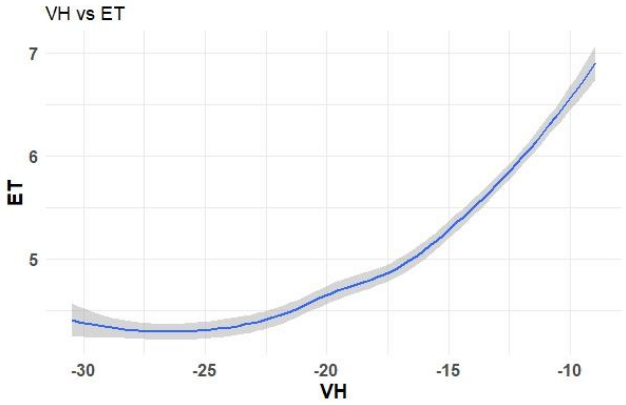

Figure 15. Partial Dependence Plot for VH and ET.

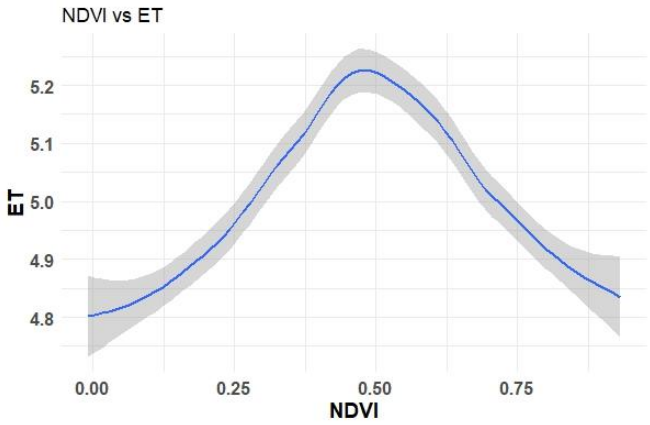

Figure 16. Partial Dependence Plot for NDVIRE1 and ET.

3.4 Random Forest Model and ET Prediction.

This section presented the outcomes of the Random Forest Model for evapotranspiration prediction for the first three scenarios as described in the method section. The section also reported an ablation analysis conducted to assess the contributions of Sentinel-1 and Sentienl-2 indices on rainfed agriculture and irrigated agriculture. This approach was essential to assess whether differences in estimated ET existed between rainfed and irrigated agriculture. The outcomes for scenarios 4, 5, 6, 7, 8, and 9 are detailed in the appendices 1, 2, 3, 4, 5, and 6.

3.5 Scenario 1: ET prediction for first scenario.

The RF model was trained with 303 samples using the six most important Sentinel-l and Sentienl-2 indices: Chlre, NDVIRE1, SAVI, NDVI, VH, and B12-SWIR2 shown in figure 10, to predict ET for all crops, all sensors. The validation of the model using 161 hold-out samples achieved (R^2 =0.67, RMSE = 1.8 $MJm^{-2}d^{-2}$, rRMSE = 0.13 $MJm^{-2}d^{-2}$, and Bias= -0.11 $MJm^{-2}d^{-2}$). The R^2 = 0.67 for the model of the first scenario indicated that approximately 67% of the variance in ET was explained by the indices from both sensors. The Root Mean Square Error (RMSE) of 1.8 $MJm^{-2}d^{-2}$ suggests that, on average, the ET estimates provided by the model were within 1.8 $MJm^{-2}d^{-2}$ of the true values. This level of accuracy is acceptable for many practical applications. Additionally, the Bias value of -0.11 $MJm^{-2}d^{-2}$ indicates that, on average, the model slightly underestimated the ET values, regardless of whether Sentinel-2 or Sentinel-1 variables were used. Though, the model shows a negative bias, the overall performance appears satisfactory. The scatterplot shown in figure 17 was generated to compare the observed ET (found on the x-axis) with the predicted ET (found on the y-axis).

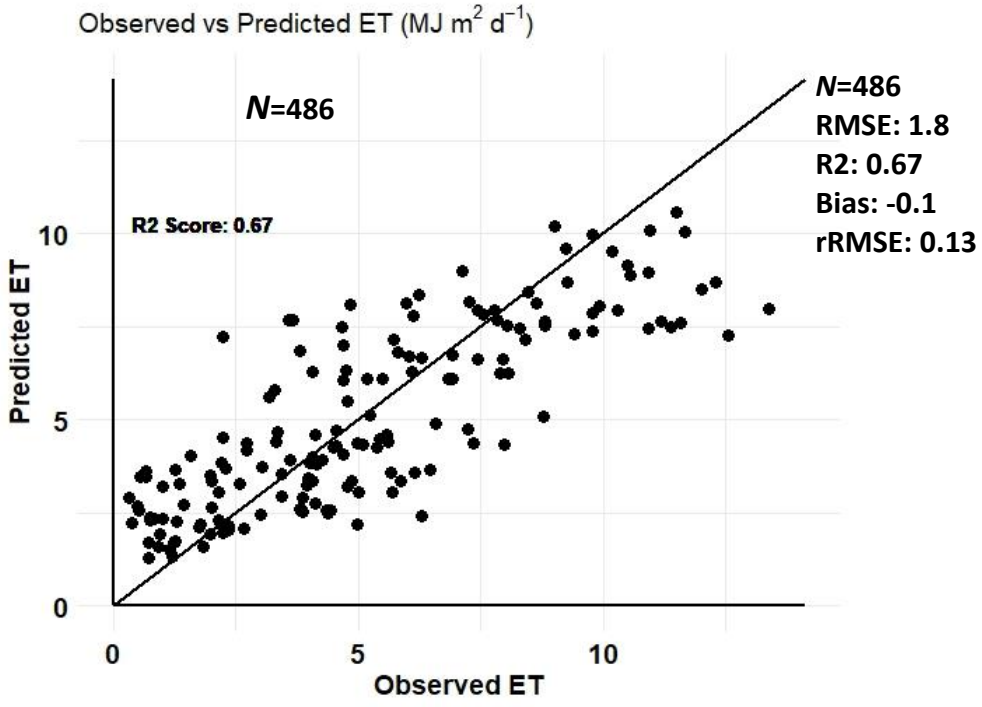

Figure 17. A scatterplot for all crops, all sensors.

3.6 ET prediction for scenario 2 and scenario 3.

The analysis conducted for scenario 2 (all crops, S-2 only) using 303 samples to train RF model revealed that the following Sentinel-2 indices: Chlre, SAVI, NDVIRE1, B12-SWIR2 and B12_SWIR2, NDVI, B8A_Red_edge4, NDVIRE2, and NDWI contributed 66% to the overall model achieving (R^2 = 0.66, RMSE = 1.9$MJm^{-2}d^{-2}$, rRMSE=0.13$MJm^{-2}d^{-2}$, and Bias = -0.11$MJm^{-2}d^{-2}$) on the 161 hold-out samples. In the case of scenario 3, (all crops, S-1 only), the following Sentinel-1indices: VV/VH, VV+VH, VH, and VV contributed 26% to the overall, model achieving (R^2 = 0.26, RMSE = 2.8$MJm^{-2}d^{-2}$, rRMSE = 0.20 $MJm^{-2}d^{-2}$, and Bias = -0.56$MJm^{-2}d^{-2}$). Overall, the results from both sensors indicated that, Sentinel-2 indices contributed significantly to the variability in ET than Sentinel-1. The scatterplots in figure 18 and figure 19 illustrates the contributions by each indices categorized by sensor.

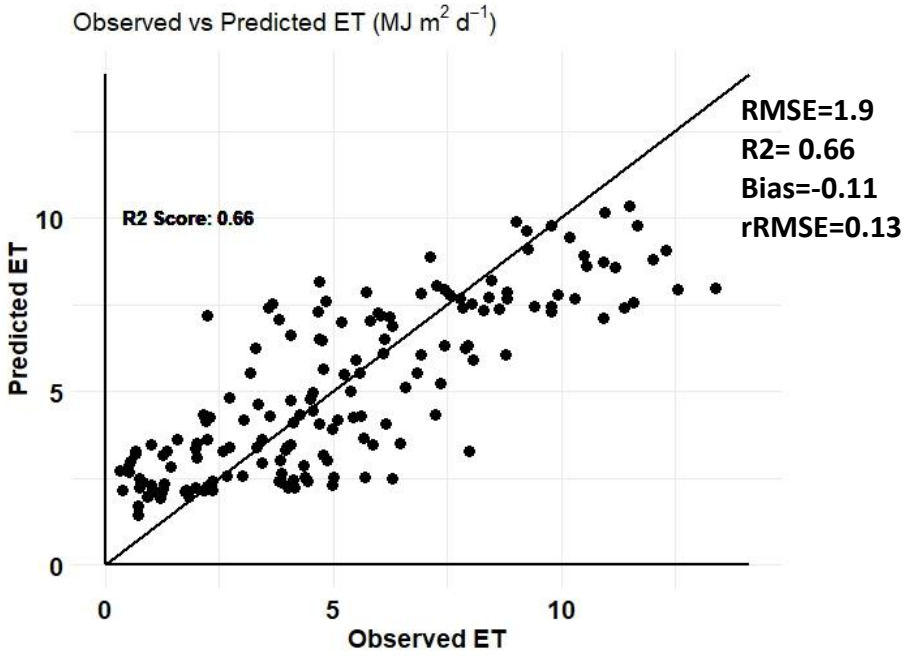

Figure 18. Scatterplot for all crops, Sentinel-2 only.

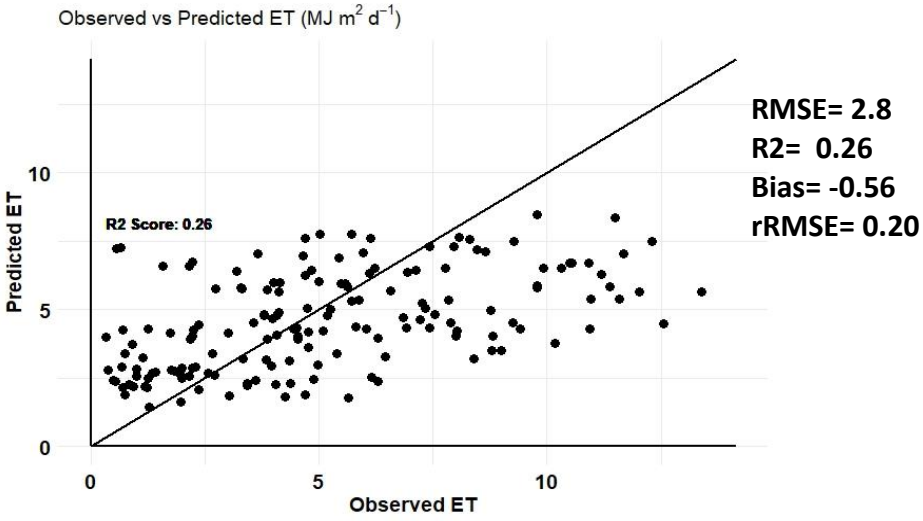

Figure 19. Scatterplot for all crops, Sentinel-1 only

3.7 ET prediction for scenario 4, 5, and 6.

For scenarios 4, 5 and 6, RF model was trained with 249 samples and validated using a hold-out sample of 137. The results for scenario 4, (rainfed, all sensors), the model explained 65% variability in ET on rainfed agriculture achieving (R^2 = 0.65, RMSE = 1.9MJm^{-2}d^{-2}=0.18, rRMSE=0.1MJm^{-2}d^{-2}, and Bias = -0.11MJm^{-2}d^{-2}). The result suggest that the predictive power of the model has reduce by 4% when validated on rainfed agriculture. Similarly, the predictive power of the model also reduced by 3% using Sentinel-2 alone. Sentinel-2 indices explained 63% of the variability in ET achieving (R^2 = 0.63, RMSE = 1.9MJm^{-2}d^{-2}, rRMSE=0.14MJm^{-2}d^{-2}, and Bias = -0.15MJm^{-2}d^{-2}). However, Sentinel-1 predictive power increase by 10% on rainfed agriculture achieving (R^2 = 0.36, RMSE = 2.6MJm^{-2}d^{-2}, rRMSE=0.19MJm^{-2}d^{-2}, and Bias = -0.61MJm^{-2}d^{-2}). The scatter plots of scenarios 4, 5 and 6, can be located in appendices 1, 2 and 3.

3.8 ET predictions for scenario 7, 8, and 9.

The RF model for scenarios 7, 8, and 9 were trained with 49 samples and validated with 29 hold-out samples. The result of scenario 7 (Irrigated, all sensors) show that, 69% of the variability in ET is better explained by Sentinel-1 and Sentinel-2 in irrigated agriculture. These result in 4% increase in its ET predictive power on irrigated agriculture after achieving (R^2=0.69, RMSE=3.3MJm^{-2}d^{-2}, rRMSE=0.24MJm^{-2}d^{-2}, and Bias = 2.2MJm^{-2}d^{-2}). The results for scenario 8 (Irrigated, S-2 only), achieved (R^2 = 0.67, RMSE = 3.3MJm^{-2}d^{-2}, rRMSE=0.25MJm^{-2}d^{-2}, and Bias = 2.3MJm^{-2}d^{-2}). For scenario 9 (Irrigated, S-1 only), the result was (R^2 = 0.29, RMSE = 4.5MJm^{-2}d^{-2}, rRMSE=0.34MJm^{-2}d^{-2}, and Bias = 2.95MJm^{-2}d^{-2}). It can be observe that Sentinel-2 indices has 4% more ET predictive power on irrigated agriculture than Rainfed. However, the predictive power of Sentinel-1 has also increased by 3%. The scatter plots for scenario 7, 8, and 9, can be found in appendices 4, 5, and 6 respectively.

4.0 DISCUSSION

This section discussed the the most important Sentinel-1 and Sentinel-2 indices, and interpreted the PDPs illustrating the relationship between ET and (Sentinel-2 and Sentinel-1 indices). The section also discussed the model performances for rainfed and irrigated agriculture and evaluated the proportion explained by Sentinel-1 indices and Sentinel-2 indices exclusively for each water regimes. Moreover, the section also addressed the study's limitations, implications and presented relevant recommendations for future research and other applications.

4.1 The most Important Sentinel-1 and Sentinel-2 indices.

One of the prime objectives of this study was to assess the most important Sentinel-1 and Sentienl-2 indices which was critical to identify the key vegetation and polarimetric indices that can precisely predict ET. This was an attempt to avoid including irrelevant and redundant variables that could potentially introduce noise and decrease the model's predictive performance. The results for the first scenarios as shown in figure 10, six (6) variables were considered as important suggesting that a more accurate estimation of ET can be achieved by incorporating variables from both Sentinel-1 and Sentinel-2. This finding greatly emphasizes

the rationale behind integrating these two data types, given their valuable and complementary information they provide. From figure 10, Chlre with %IncMSE of 27.18 is considered the most important, meaning that RF model cannot predict ET with high accuracy when Chlre is missing. This can be attributed to Chlre sensitivity to changes in chlorophyll and leaf water contents (Gitelson et al., 2003). Chlorophyll is essential for photosynthesis, the process through which plants convert sunlight into energy and produce oxygen. The photosythetic processes have a direct connection with water loss from plants into the atmosphere through stomatal openings. This water loss is closely linked to the overall evapotranspiration process. This finding aligned with previous reseach by Haboudane et al (2002), who underscore Chlre to be significant and essential for prediction of crop chlorophyll content. The B12_SWIR2 representing band 12 shortwave infra-red region of the electromagnetic spectrum was also selected, which is known for its sensivity to moisture contents of soil and vegetation. The selection of B12_SWIR reaffirm our knowledge of the pivotal role chlorophyll and water content plant in the processes of evapotranspiration. Similar result was found by Liu et al. (2021), who found B12_SWIR to be significant for estimating soil moisture in agriculture fields. Another significant Sentinel-2 vegetation indices selected was NDVIRE1. This index is specifically designed to capture chlorophyll information in vegetation. Healthy plants with abundant chlorophyll content tend to have vigorous growth, which leads to increased transpiration, a significant component of ET (Evangelides & Nobajas, 2020). Soil-Adjusted Vegetation Index was selected as the fourth most important variable. The significance of including the SAVI for ET estimation lies in its capacity to address soil brightness and differentiate between vegetation and soil signal, thereby contributing to improved ET estimation (Alam et al., 1996). The VH polarization from Sentinel-1 was the only variables selected under the first scenario as important for ET estimate. VH polarization was selected because of its sensitivity to vegetation cover and structure. VH can capture variations in vegetations density, height, and canopy structure, which are essential factors influencing transpiration and overall ET. Similarly, VH polarization can penetrate canopy cover influenced by its volume scattering characteristics. This allows it to captures information regarding soil surface and upper canopy, providing valuable insights into the vegetation transpiration and soil evaporation (Harfenmeister et al., 2019). By using VH polarization backscatter, the study by Schlund & Erasmi (2020b), demonstrates the importance of VH for crop phenology, which is closely related to vegetation water intake and transpiration. Finally, NDVI was also selected as important for ET estimate. Although NDVI is commonly used in remote sensing and environmental studies, its lower ranking among the six selected variables for ET estimation agree with previous research. For instance, Evangelides & Nobajas, (2020), suggested that previously selected vegetation indices have specific capabilities for capturing particular vegetation characteristics, allowing them to outperform NDVI in estimating ET. Moreover, Meng et al (2013), added that NDVI is primarily sensitive to variations in vegetation density and greenness, which might limit its ability to capture other important factors influencing evapotranspiration, such as soil moisture and leaf water content. Furthermore, NDVI has a saturation point beyond which changes in vegetation density and greeness may not influence ET processes. Nevertheless, its simplicity and its role as a valuable vegetation health indicator are some of the reasons it might be choosen for ET estimate. To this end, the initial hypothesis posited that, Red edge and Near infra red bands from Sentinel-2 would be the most important predictors giving their sensitivity to transpiration, whiles Sentinel-1 backscatter would be more important, but less so given its sensitivity to soil evaporation. However, the findings of the study lead to the rejection of the initial hypothesis.

4.2 Partial Dependence Plots.

The partial dependence plots displayed in figures 11 to 16 reveal varying degrees of relationship between the variables and ET. Whiles some plots exhibit a linear trend, others demonstrate a degree of linearity but saturate at certain points. For instance, in figure 11, ET increases when Chlre was 0.3, but begins to saturates after after ET reaches 6.7 and Chlre reaches 3.1. This is because Chlre reached saturation point beyond which additional increases in Chlre no longer impact ET process. Similarly observation by (Darvishzadeh et al., 2009; Delegido et al., 2011), who obseved a linear relationship between Chlre and the estimations of leaf area index and chlorophyll content, a major parameter for photosynthesis, which relate to transpiration the largest component of ET.

In the case of B12_SWIR as illustrated in figure 12, the PDP revealed that ET has a continous linear trend with B12_SWIR. This trend could be attributed to B12_SWIR sensitivity to soil and vegetation moisture (Liu et al., 2021), resulting in a rise even in the absence of vegetation. Mandal et al. (2018), further reaffirm such occurences, stating that, such phenomenon can be attributed to the use of machines to harvest crops living large amount of crop residues on the field. As a results, the existence of crop residues leads to an increase B12-SWIR due to its ability to detect soil moisture and chlorophyll signals from the remnants (Mandal et al., 2018).

NDVIRE1, as highlighted by Evangelides & Nobajas (2020), is sensitive to changes in chlorophyll content and vegetation density. The PDP for NDVIRE1 shows that as vegetation becomes healthier and denser, they tend to enhance capacity for transpiration ultimately leading to increased ET. From figure 13, it can be observed that, ET began to increase at 0.2 when leaf of crops have shoot up, but increases as crops reached maturity at 0.7 and begin to fall. During this stage of the plant, transpiration rate of the plants decreases as they prioritized reproduction over growth. This can also relates to crop adaptation to water stress. Crops could close their stomata to reduce water loss during time of limited water availability (FAO, 2002). Additionally, healthier canopy might have more dense foliage, which can lead to increased shading of the soil surface. Shaded soil surfaces can reduce soil evaporation, contributing to lower overall evapotranspiration.
The PDP for SAVI demonstrates a similar trend to B12_SWIR. However, it reveals that ET rate slows down once the crops reach full maturity. As illustrated by the PDP, as SAVI increase, it implies increasing growth and development of crops, leading to a corresponding increase in ET. However, ET values decreases at 0.5 when the crop reaches its maximum growth, slowing down the rate of ET. Farg et al. (2012) also reported comparable results, stating that when crop reaches maturity, there is a reduced demand for water due to the stabilization of physiological processes. Consequently, the rate of water loss through transpiration begins to decrease, leading to the observed slowdown in ET.

The VH polarization PDP in Figure 15 shows that VH and ET increase at a slow rate during the initial stages of crop development. The slow increase in VH polarization is likely due to the early growth phases, where the vegetation is still establishing and the canopy density is not fully developed. As the crops continue to grow and their leaves and branches expand, the VH backscatter increases resulting in a continous increase in ET. This finding is consistent with the results from Schlund & Erasmi's (2020c) study on winter wheat. In their study, they observed that VH backscatter did not decrease even after the crops had been harvested. This is because the crop stubble left on the field after harvest produces a backscatter signal similar to that of fully grown crops. Hence, the backscatter levels do not decrease significantly after

harvesting (Schlund & Erasmi, 2020c). moreover, the pattern observed can also be attributed to longer growing season with a large proportion of late-planted crops, such as corn and soybeans. Again, it is essential to consider that this analysis was conducted across four different crop fields, and the practices adopted after harvesting varied among these fields. Therefore, to validate the underlying reasons for this phenomenon, field survey should be conducted in future studies as proposed by (M Bouman & J van Kasteren, 1990).

The PDP of NDVI has shown a different pattern, ET increases even when NDVI was 0.0. This phenomenon is perhaps because crops were at their early stages of development, which suggests that there is greater surface area available for soil evaporation leading to an increase in ET. The saturation of ET when NDVI is 0.48 is related to the saturation point of NDVI itself. This means that NDVI becomes less sensitive to changes in vegetaion density beyond 0.5, stabelizing the relatioship between ET and NDVI. Subsequently, the decrease in ET as NDVI reaches 0.75 is consistent with annual crops under rainfed agriculture, where water decrease monotonously through out the growing season, resulting in general water deficit, neccitating the closure of stomata walls by crops to prevent water loss.

4.3 Performance of Random Forest model.

The study has evaluated the predictive ability of Sentinel-1 and Sentinel-2 indices to estimate ET in both rainfed and irrigated agriculture. The result revealed that Sentinel-2 indices explained more ET variability in all cases. While Sentinel-1 alone did not provide a strong explanation for the variations in ET. Though it increase in its explanatory power on irrigated as expected , it was lower compared to its explanatory power on rainfed agriculture. This could attributed to the sample size used in training the model which may not be representative enough. Congalton (2001), underscore this assertions by stating that, larger sample size per class provides more representative information for constructing error matrix, enhancing the reliability of the accuracy assessment and subsequently improving the model's predictive power. Moreover, Sentinel-2 might explain more variability in ET than Sentinel-1 because, optical imagery from Sentinel-2 enables direct observation of vegetation chlorophyll and water contents, which are proxy to photosynthetic activities of plants, a critical components of ET process. Another reason stated by Nasseri et al (2023) was that, Sentinel-2 imagery can provide data on land surface temperature, which is closely related to ET. Increase land surface temperature levels means increase CO_2 (Hatfield & Dold, 2019). Plants take in CO_2 for photosynthesis, but also allow water to escape through transpiration. In general, the dominance of Sentinel-2 over Sentinel-1 is because Sentinel-2 is sensitive to vegetation density, health and greenness. These factors are directly related to transpiration the largest component of ET. Sentinel-1 on the other hand is sensitive to soil moisture content which relates to soil evaporation the second largest component of ET. Its ability to capture soil moisture is limited when the canopy covers the land surface as transpiration take precedence.

Moreover, the results has shown a decline in ET over rainfed agriculture by 2% but an increase by 2% on irrigated agriculture. This phenomenon is likely due to water stress. According to Yang et al (2018), when there is limited rainfall, plants experience water stress, which can lead to stomatal closure. Stomata, the tiny pores on leaves, regulate both CO_2 uptake for photosynthesis and water vapor loss through transpiration. In response to water stress, plants tend to close their stomata to conserve water, reducing the rate of transpiration and, consequently, ET. Cammalleri et al (2014), found similar results, stating that, on irrigated agriculture, water is spatially continuous, resulting in continuous movement of

moisture in plants. With access to sufficient water, plants can maintain open stomata and continue transpiring water vapor actively. Higher transpiration rates contribute to increased ET levels.

However, caution must be taking in explaining the results for irrigated agriculture due to low sample size used for training the model. A larger number of samples size as mentioned by Khalilzadeh & Tasci (2017), leads to more accurate parameter estimates and increased statistical power, enabling researchers to detect smaller effects with greater confidence. Given the bias observed in the results for irrigated agriculture, it is important to consider that a relatively limited dataset could introduce potential biases and might not adequately capture the complexity and variability of ET estimation in irrigated agriculture. Therefore, while the result is promising, further validation with larger datasets is recommended to ensure the model's robustness and reliability for broader applications.

4.6 Limitations.

The results from the integration of Sentinel-1 and Sentinel-2 data for estimating evapotranspiration in rainfed and irrigated agriculture has shown great promise. However, it is crucial to consider certain aspect of the study that requires further consideration when applying the findings to other regions. Future research should address these limitations and conduct further validations to enhance the robustness and applicability of the integrated remote sensing approach for evapotranspiration estimation.

One such limitation was the limited number of samples for some crops for the analysis. As stated by (Ma et al., 2022), the size of dataset can significantly impact the reliability and the general rebustness of the results. A relatively small dataset may lead to potential biases, and may not fully capture the inherent variability in ET for the crops for this analysis. To mitigate this limitation, future research could consider collecting more data points, which could likely lead to more robust model training, validation, and better representaion of the true ET variablitity.

An additional, the analysis has been able to explain why Sentinel-2 explains ET better on rainfed and irrigated, but lack explanation on the partitioning of ET into soil evaporation and canopy transpiration which is a source of uncertaintity in this analysis. In future research, specific methods like surface energy balace model, and eddy covariance method would be required to partition ET into its components. Only then can we confidently conclude that Sentinel-2 primarily explains the transpiration component of ET, the largest component of ET, while Sentinel-1 accounts for soil evaporation, the second-largest component of ET.

Furthermore, an aspect that needs further consideration is the manner in which the study defined the start and end of seasons, employing months rather than precise dates to define the start and end of growing seasons. This approach affects the accuracy of ET estimate for Senitinel-1 in all cases, which the study expect to be more useful but apparently does not compete with Sentinel-2. In future studies, field survey should be conducted as proposed by (M Bouman & J van Kasteren (1990), on the exact dates but not excluding the management paractices that occurs on the fields of each crops. Alternatively, regular updates on farm management practices from Principal Investigators on each site could help overcome this challenge.

Moreover, the current study was undertaken in regions where sentinel-2 target data were rarely obstructed by clouds, enabling the collection of reflectance values. However, if similar analysis were conducted in regions where cloud cover is pravalent all year-round, overcoming the shortage of data from Sentinel-2 may present a substantial challenge.

4.7 Implications.

The estimation of ET in both rainfed and irrigated agriculture has significant important implications for agricultural planning and water management. Farmers and stakeholders can make informed decisions, by practicing precision irrigation techniques that reduce water wastage and enhance overall water use efficiency. This can increase crop production and ensure the management of water resources.

Moreover, the findings in this study highlighted the significance of integrating data from Sentinel-1 and Sentinel-2 sensors for ET estimation. In future, the identified important variables can guide the selection of input features for other models, potentially improving their predictive accuracy.

Furthermore, future research could explore the potential, capabilities, and complementary information provided by Sentinel-1 and Sentinel-2 beyond ET estimation. One promising avenue is the application of this integrated approach in drought modeling and assessment. Drought is complex phenomenon with far-reaching socio-economic and environmental implications, making its accurate prediction and monitoring of utmost importance.

4.8 Recommendations.

Building on the outcomes of this study, it is advised to consider the following recommendations in order to amplify the practical application and significance of the research:

In subsequent research, it would be valuable for researchers to investigate the feasibility and effectiveness of integrating Sentienl-1 and Sentienl-2 on smaller-scale farms, particularly in regions such as Africa where small size farms are prevalent. By conducting further research in this diverse geographical contexts and with various crop varieties, researchers can ascertain the broader applicability of estimating crop water requirements.

In future study, researchers should collect more data points for each crops. Moreover, relevant information on farm management practices before and after harvest should be collected from principal investigation to enhance the interpretation of results. This can be achieve by collaborating with site PIs to facilitate the collection of such information, enabling a more comprehensive validation of random forest model for ET estimation and enhancing the reliability and interpretation of the results.

5.0 CONCLUSION

Global ET estimate is essential for sustainable water used on both local and regional scale, particularly in advancing precise irrigation practices to bolster agricultural productivity. However, inputs and model uncertainties limits the estimation of ET on a global scale. Using quality data that strike the balance between temporal and spatial resolution using machine learning algorithms provides a better alternatives. These study therefore demonstrated the significance of integrating Sentinel-1 (sensitive to soil moisture and canopy structure) and Sentinel-2 (sensitive to canopy transpiration) for ET estimation on irrigated agriculture. The analysis was conducted on two water regimes, which was necessary to understand if the predictive performance of the Random Forest (RF) model would differ.

The study has successfully predicted ET on rainfed and irrigated agriculture, revealing that RF model explained more variability in ET on irrigated agriculture than rainfed agriculture. This was expected due to the continous availability of moisture for plant transpiration on rainfed agriculture. The lower performance on rainfed agriculture on the other hand was due to limited was supply, which force crops to adapt by closing their stomata walls, hence reducing ET. Similarly, Sentinel-2 explained significant variability in ET than Sentinel-1, suggesting that Sentinel-2 vegetation indices cannot explain ET variability in isolation. The studies further discovered that the most significant variable selected was chlorophyll red-edge index (Chlre), which is sentive to chlorophyll and water contents of vegetations. These vegetation parameters relates to photosynthesis. The photosythetic processes have a direct connection with water loss from plants into the atmosphere through stomatal openings. Moreover, NDVI, a commonly used indicator in various applications, ranked the lowest among the top six variables. This outcome was linked to the saturation point of NDVI, indicating a stage where further vegetation growth no longer leads to an increase in evapotranspiration.

Though, the integration of both sensors using machine learning method has been able to explain why Sentinel-2 explains ET better on rainfed and irrigated, the study lack explanation on the partitioning of ET into soil evaporation and canopy transpiration which is a source of uncertaintity. Overall, the estimation of global evapotranspiration ET holds paramount importance for ensuring sustainable water management practices at both local and regional scales. This is particularly crucial for enhancing precise irrigation management that could increased agricultural productivity.

6.0 LIST OF REFERENCES

(United Nations). (2015). *Facing the challenges : case studies and indicators : UNESCO's contribution to the United Nations world water development report 2015.*

Alam, M. J., Rahman, K. M., Asna, S. M., Muazzam, N., Ahmed, I., & Chowdhury, M. Z. (1996). Comparative studies on IFAT, ELISA & DAT for serodiagnosis of visceral leishmaniasis in Bangladesh. *Bangladesh Medical Research Council Bulletin*, *22*(1), 27–32.

Anderson, M. C., Allen, R. G., Morse, A., & Kustas, W. P. (2012). Use of Landsat thermal imagery in monitoring evapotranspiration and managing water resources. *Remote Sensing of Environment*, *122*, 50–65. https://doi.org/10.1016/j.rse.2011.08.025

Badgley, G., Fisher, J. B., Jiménez, C., Tu, K. P., & Vinukollu, R. (2015). On uncertainty in global terrestrial evapotranspiration estimates from choice of input forcing datasets. *Journal of Hydrometeorology*, *16*(4), 1449–1455. https://doi.org/10.1175/JHM-D-14-0040.1

Becker, F., & Choudhury, B. J. (1988). Relative sensitivity of normalized difference vegetation Index (NDVI) and microwave polarization difference Index (MPDI) for vegetation and desertification monitoring. *Remote Sensing of Environment*, *24*(2), 297–311. https://doi.org/10.1016/0034-4257(88)90031-4

Belgiu, M., & Dra, L. (2016). *ISPRS Journal of Photogrammetry and Remote Sensing Random forest in remote sensing : A review of applications and future directions ˇ gut*. *114*, 24–31. https://doi.org/10.1016/j.isprsjprs.2016.01.011

Belgiu, M., & Drăgu, L. (2016). Random forest in remote sensing: A review of applications and future directions. *ISPRS Journal of Photogrammetry and Remote Sensing*, *114*, 24–31. https://doi.org/10.1016/j.isprsjprs.2016.01.011

Biggs, T. W., Petropoulos, G. P., Velpuri, N. M., Marshall, M., Glenn, E. P., Nagler, P., & Messina, A. (2015). Remote sensing of actual evapotranspiration from croplands. *Remote Sensing of Water Resources, Disasters, and Urban Studies*, *3*, 59–99. https://doi.org/10.1201/b19321

Breiman, L. (2001). *Random Forests*. *45*, 5–32.

Cammalleri, C., Anderson, M. C., Gao, F., Hain, C. R., & Kustas, W. P. (2014). Mapping daily evapotranspiration at field scales over rainfed and irrigated agricultural areas using remote sensing data fusion. *Agricultural and Forest Meteorology*, *186*, 1–11. https://doi.org/10.1016/j.agrformet.2013.11.001

Chapin, S., Matson, P., & Harold. (2006). *Principles of Terrestrial Ecosystem Ecology - F Stuart Chapin III, Pamela A. Matson, Harold A. Mooney - Google Books*. https://books.google.nl/books?id=shsBCAAAQBAJ&printsec=frontcover&source=gbs_ge_summary_r&cad=0#v=onepage&q&f=false

Chen, J., Jönsson, P., Tamura, M., Gu, Z., Matsushita, B., & Eklundh, L. (2004). A simple method for reconstructing a high-quality NDVI time-series data set based on the Savitzky-Golay filter. *Remote Sensing of Environment*, *91*(3–4), 332–344. https://doi.org/10.1016/j.rse.2004.03.014

Cleugh, H. A., Leuning, R., Mu, Q., & Running, S. W. (2007). Regional evaporation estimates from flux tower and MODIS satellite data. *Remote Sensing of Environment*, *106*(3), 285–304. https://doi.org/10.1016/J.RSE.2006.07.007

Congalton, R. G. (2001). Accuracy assessment and validation of remotely sensed and other spatial information. *International Journal of Wildland Fire*, *10*(3–4), 321–328. https://doi.org/10.1071/wf01031

Darvishzadeh, R., Atzberger, C., Skidmore, A. K., & Abkar, A. A. (2009). Leaf Area Index derivation from hyperspectral vegetation indicesand the red edge position. *International Journal of Remote Sensing*, *30*(23), 6199–6218. https://doi.org/10.1080/01431160902842342

Debats, S. R., Luo, D., Estes, L. D., Fuchs, T. J., & Caylor, K. K. (2016). A generalized computer vision approach to mapping crop fields in heterogeneous agricultural landscapes. *Remote Sensing of Environment*, *179*, 210–221. https://doi.org/10.1016/J.RSE.2016.03.010

Delegido, J., Verrelst, J., Alonso, L., & Moreno, J. (2011). Evaluation of sentinel-2 red-edge bands for empirical estimation of green LAI and chlorophyll content. *Sensors*, *11*(7), 7063–7081.

https://doi.org/10.3390/s110707063
Devries, B., Huang, C., Armston, J., Huang, W., Jones, J. W., & Lang, M. W. (2020). *Hydrologic Remote Sensing Branch*. https://doi.org/10.1016/j.rse.2020.111664
El-Baroudy, I., Elshorbagy, A., Carey, S. K., Giustolisi, O., & Savic, D. (2010). Comparison of three data-driven techniques in modelling the evapotranspiration process. *Journal of Hydroinformatics*, *12*(4), 365–379. https://doi.org/10.2166/hydro.2010.029
El Hachimi, J., El Harti, A., Lhissou, R., Ouzemou, J.-E., Chakouri, M., & Jellouli, A. (2022). Combination of Sentinel-2 Satellite Images and Meteorological Data for Crop Water Requirements Estimation in Intensive Agriculture. *Agriculture*, *12*(8), 1168. https://doi.org/10.3390/agriculture12081168
ESA - Sentinel-2. (n.d.). Retrieved August 17, 2023, from https://www.esa.int/Applications/Observing_the_Earth/Copernicus/Sentinel-2
Evangelides, C., & Nobajas, A. (2020). Red-Edge Normalised Difference Vegetation Index (NDVI705) from Sentinel-2 imagery to assess post-fire regeneration. *Remote Sensing Applications: Society and Environment*, *17*. https://doi.org/10.1016/j.rsase.2019.100283
Falge, E., Baldocchi, D., Olson, R., Anthoni, P., Aubinet, M., Bernhofer, C., Burba, G., Ceulemans, R., Clement, R., Dolman, H., Granier, A., Gross, P., Grünwald, T., Hollinger, D., Jensen, N. O., Katul, G., Keronen, P., Kowalski, A., Lai, C. T., … Wofsy, S. (2001). Gap filling strategies for defensible annual sums of net ecosystem exchange. *Agricultural and Forest Meteorology*, *107*(1), 43–69. https://doi.org/10.1016/S0168-1923(00)00225-2
FAO. (2002). *Deficit Irrigation Practices*. https://www.fao.org/3/y3655e/y3655e03.htm
Farg, E., Arafat, S. M., Abd El-Wahed, M. S., & El-Gindy, A. M. (2012). Estimation of Evapotranspiration ETc and Crop Coefficient K c of Wheat, in south Nile Delta of Egypt Using integrated FAO-56 approach and remote sensing data. *Egyptian Journal of Remote Sensing and Space Science*, *15*(1), 83–89. https://doi.org/10.1016/j.ejrs.2012.02.001
Fernández-Manso, A., Fernández-Manso, O., & Quintano, C. (2016). SENTINEL-2A red-edge spectral indices suitability for discriminating burn severity. *International Journal of Applied Earth Observation and Geoinformation*, *50*, 170–175. https://doi.org/10.1016/j.jag.2016.03.005
Fisher, J. B., Melton, F., Middleton, E., Hain, C., Anderson, M., Allen, R., McCabe, M. F., Hook, S., Baldocchi, D., Townsend, P. A., Kilic, A., Tu, K., Miralles, D. D., Perret, J., Lagouarde, J. P., Waliser, D., Purdy, A. J., French, A., Schimel, D., … Wood, E. F. (2017). The future of evapotranspiration: Global requirements for ecosystem functioning, carbon and climate feedbacks, agricultural management, and water resources. *Water Resources Research*, *53*(4), 2618–2626. https://doi.org/10.1002/2016WR020175
Fisher, J. B., Tu, K. P., & Baldocchi, D. D. (2008). Global estimates of the land-atmosphere water flux based on monthly AVHRR and ISLSCP-II data, validated at 16 FLUXNET sites. *Remote Sensing of Environment*, *112*(3), 901–919. https://doi.org/10.1016/j.rse.2007.06.025
Frampton, W. J., Dash, J., Watmough, G., & Milton, E. J. (2013). Evaluating the capabilities of Sentinel-2 for quantitative estimation of biophysical variables in vegetation. *ISPRS Journal of Photogrammetry and Remote Sensing*, *82*, 83–92. https://doi.org/10.1016/j.isprsjprs.2013.04.007
Friedman, J. H. (n.d.). *No Tit.אלצבן*. https://www.ptonline.com/articles/how-to-get-better-mfi-results
Genuer, R., Poggi, J. M., & Tuleau-Malot, C. (2015). VSURF: An R package for variable selection using random forests. *R Journal*, *7*(2), 19–33. https://doi.org/10.32614/rj-2015-018
Gitelson, A. A., Gritz, Y., & Merzlyak, M. N. (2003). Relationships between leaf chlorophyll content and spectral reflectance and algorithms for non-destructive chlorophyll assessment in higher plant leaves. *Journal of Plant Physiology*, *160*(3), 271–282. https://doi.org/10.1078/0176-1617-00887
Gitelson, A. A., Merzlyak, M. N., & Lichtenthaler, H. K. (1996). Detection of red edge position and chlorophyll content by reflectance measurements near 700 nm. *Journal of Plant Physiology*, *148*(3–4), 501–508. https://doi.org/10.1016/S0176-1617(96)80285-9

Glenn, E. P., Nagler, P. L., & Huete, A. R. (2010). Vegetation Index Methods for Estimating Evapotranspiration by Remote Sensing. *Surveys in Geophysics*, *31*(6), 531–555. https://doi.org/10.1007/S10712-010-9102-2/FIGURES/5

Gorrab, A., Ameline, M., Albergel, C., & Baup, F. (2021). Use of sentinel-1 multi-configuration and multi-temporal series for monitoring parameters of winter wheat. *Remote Sensing*, *13*(4), 1–19. https://doi.org/10.3390/rs13040553

Haboudane, D., Miller, J. R., Tremblay, N., Zarco-Tejada, P. J., & Dextraze, L. (2002). Integrated narrow-band vegetation indices for prediction of crop chlorophyll content for application to precision agriculture. *Remote Sensing of Environment*, *81*(2–3), 416–426. https://doi.org/10.1016/S0034-4257(02)00018-4

Hadadi, F., Moazenzadeh, R., & Mohammadi, B. (2022). Estimation of actual evapotranspiration: A novel hybrid method based on remote sensing and artificial intelligence. *Journal of Hydrology*, *609*, 127774. https://doi.org/10.1016/j.jhydrol.2022.127774

Hamrell, M. R. (2014). What is an IND? *FDA Regulatory Affairs: Third Edition*, *266*(April 1995), 41–76. https://doi.org/10.3109/9781420073553-3

Harfenmeister, K., Spengler, D., & Weltzien, C. (2019). Analyzing temporal and spatial characteristics of crop parameters using Sentinel-1 backscatter data. *Remote Sensing*, *11*(13), 1–30. https://doi.org/10.3390/rs11131569

Hatfield, J. L., & Dold, C. (2019). Water-use efficiency: Advances and challenges in a changing climate. *Frontiers in Plant Science*, *10*(February), 1–14. https://doi.org/10.3389/fpls.2019.00103

Hu, X., Shi, L., Lin, G., & Lin, L. (2021a). Comparison of physical-based, data-driven and hybrid modeling approaches for evapotranspiration estimation. *Journal of Hydrology*, *601*, 126592. https://doi.org/10.1016/j.jhydrol.2021.126592

Hu, X., Shi, L., Lin, G., & Lin, L. (2021b). Comparison of physical-based, data-driven and hybrid modeling approaches for evapotranspiration estimation. *Journal of Hydrology*, *601*, 126592. https://doi.org/10.1016/J.JHYDROL.2021.126592

Hu, Y., Buttar, N. A., Tanny, J., Snyder, R. L., Savage, M. J., & Lakhiar, I. A. (2018). Surface Renewal Application for Estimating Evapotranspiration: A Review. *Advances in Meteorology*, *2018*. https://doi.org/10.1155/2018/1690714

Ito, A., Nishina, K., Christopher, P., Reyer, O., Orth, R., Seneviratne, S. I., Rosenzweig, C., Arnell, N. W., Wartenburger, R., Seneviratne, S. I., Hirschi, M., Chang, J., & Ciais, P. (2018). Evapotranspiration simulations in ISIMIP2a — Evaluation of spatio-temporal characteristics with a comprehensive ensemble of independent datasets. *Environmental Research Letters*.

Jiménez, C., Prigent, C., Mueller, B., Seneviratne, S. I., McCabe, M. F., Wood, E. F., Rossow, W. B., Balsamo, G., Betts, A. K., Dirmeyer, P. A., Fisher, J. B., Jung, M., Kanamitsu, M., Reichle, R. H., Reichstein, M., Rodell, M., Sheffield, J., Tu, K., & Wang, K. (2011). Global intercomparison of 12 land surface heat flux estimates. *Journal of Geophysical Research Atmospheres*, *116*(2). https://doi.org/10.1029/2010JD014545

Khalilzadeh, J., & Tasci, A. D. A. (2017). Large sample size, significance level, and the effect size: Solutions to perils of using big data for academic research. *Tourism Management*, *62*, 89–96. https://doi.org/10.1016/j.tourman.2017.03.026

Khan, M. R., de Bie, C. A. J. M., van Keulen, H., Smaling, E. M. A., & Real, R. (2010). Disaggregating and mapping crop statistics using hypertemporal remote sensing. *International Journal of Applied Earth Observation and Geoinformation*, *12*(1), 36–46. https://doi.org/10.1016/j.jag.2009.09.010

Kingston, D. G., Todd, M. C., Taylor, R. G., Thompson, J. R., Arnell, N. W., Kingston, D. G., Todd, M. C., Taylor, R. G., Thompson, J. R., & Arnell, N. W. (2009). Uncertainty in the estimation of potential evapotranspiration under climate change. *Geophysical Research Letters*, *36*(20), 20403. https://doi.org/10.1029/2009GL040267

Kumar, M., Raghuwanshi, N. S., Singh, R., Wallender, W. W., & Pruitt, W. O. (2002). Estimating

Evapotranspiration using Artificial Neural Network. *Journal of Irrigation and Drainage Engineering*, *128*(4), 224–233. https://doi.org/10.1061/(ASCE)0733-9437(2002)128:4(224)

Lawrence, R. L., Wood, S. D., & Sheley, R. L. (2006). Mapping invasive plants using hyperspectral imagery and Breiman Cutler classifications (randomForest). *Remote Sensing of Environment*, *100*(3), 356–362. https://doi.org/10.1016/j.rse.2005.10.014

Liou, Y. A., & Kar, S. K. (2014). Evapotranspiration estimation with remote sensing and various surface energy balance algorithms-a review. *Energies*, *7*(5), 2821–2849. https://doi.org/10.3390/en7052821

Liu, Y., Qian, J., & Yue, H. (2021). Comprehensive Evaluation of Sentinel-2 Red Edge and Shortwave-Infrared Bands to Estimate Soil Moisture. *IEEE Journal of Selected Topics in Applied Earth Observations and Remote Sensing*, *14*, 7448–7465. https://doi.org/10.1109/JSTARS.2021.3098513

Lowder, S. K., Skoet, J., & Raney, T. (2016). The Number, Size, and Distribution of Farms, Smallholder Farms, and Family Farms Worldwide. *World Development*, *87*, 16–29. https://doi.org/10.1016/j.worlddev.2015.10.041

Lu, D., Chen, Q., Wang, G., Liu, L., Li, G., & Moran, E. (2016). A survey of remote sensing-based aboveground biomass estimation methods in forest ecosystems. *International Journal of Digital Earth*, *9*(1), 63–105. https://doi.org/10.1080/17538947.2014.990526

M Bouman, B. A., & J van Kasteren, H. W. (1990). *Ground-Based X-Band (3-cm Wave) Radar Backscattering of Agricultural Crops. II. Wheat, Barley, and Oats; the Impact of Canopy Structure*. *34*, 107–118.

Ma, C., Johansen, K., & McCabe, M. F. (2022). Monitoring Irrigation Events and Crop Dynamics Using Sentinel-1 and Sentinel-2 Time Series. *Remote Sensing*, *14*(5), 1–21. https://doi.org/10.3390/rs14051205

Mandal, D., Kumar, V., Bhattacharya, A., Rao, Y. S., Siqueira, P., & Bera, S. (2018). Sen4Rice: A processing chain for differentiating early and late transplanted rice using time-series sentinel-1 SAR data with google earth engine. *IEEE Geoscience and Remote Sensing Letters*, *15*(12), 1947–1951. https://doi.org/10.1109/LGRS.2018.2865816

Marshall, M., Thenkabail, P., Biggs, T., & Post, K. (2016). Hyperspectral narrowband and multispectral broadband indices for remote sensing of crop evapotranspiration and its components (transpiration and soil evaporation). *Agricultural and Forest Meteorology*, *218–219*, 122–134. https://doi.org/10.1016/j.agrformet.2015.12.025

Marshall, M., Tu, K., & Andreo, V. (2020). On Parameterizing Soil Evaporation in a Direct Remote Sensing Model of ET: PT-JPL. *Water Resources Research*, *56*(5), 1–18. https://doi.org/10.1029/2019WR026290

Maya Gopal, P. S., & Bhargavi, R. (2019). Performance Evaluation of Best Feature Subsets for Crop Yield Prediction Using Machine Learning Algorithms. *Applied Artificial Intelligence*, *33*(7), 621–642. https://doi.org/10.1080/08839514.2019.1592343

Meng, J., Du, X., & Wu, B. (2013). Generation of high spatial and temporal resolution NDVI and its application in crop biomass estimation. *International Journal of Digital Earth*, *6*(3), 203–218. https://doi.org/10.1080/17538947.2011.623189

Moorhead, J. E., Marek, G. W., Gowda, P. H., Lin, X., Colaizzi, P. D., Evett, S. R., & Kutikoff, S. (2019). Evaluation of evapotranspiration from eddy covariance using large weighing lysimeters. *Agronomy*, *9*(2), 1–17. https://doi.org/10.3390/agronomy9020099

Moreira, A., Prats-Iraola, P., Younis, M., Krieger, G., Hajnsek, I., & Papathanassiou, K. P. (2013). A tutorial on synthetic aperture radar. *IEEE Geoscience and Remote Sensing Magazine*, *1*(1), 6–43. https://doi.org/10.1109/MGRS.2013.2248301

Mutanga, O., Adam, E., & Cho, M. A. (2012). High density biomass estimation for wetland vegetation using worldview-2 imagery and random forest regression algorithm. *International Journal of Applied Earth Observation and Geoinformation*, *18*(1), 399–406. https://doi.org/10.1016/j.jag.2012.03.012

Nasirzadehdizaji, R., Sanli, F. B., Abdikan, S., Cakir, Z., Sekertekin, A., & Ustuner, M. (2019). Sensitivity analysis of multi-temporal Sentinel-1 SAR parameters to crop height and canopy coverage. *Applied Sciences (Switzerland)*, *9*(4). https://doi.org/10.3390/app9040655

Nasseri, S., Farhadi Bansouleh, B., & Azari, A. (2023). Estimation of land surface temperature in agricultural lands using Sentinel 2 images: A case study for sunflower fields. *Irrigation and Drainage*, *January*, 796–806. https://doi.org/10.1002/ird.2802

Norman, J. M., Kustas, W. P., & Humes, K. S. (1995). Source approach for estimating soil and vegetation energy fluxes in observations of directional radiometric surface temperature. *Agricultural and Forest Meteorology*, *77*(3–4), 263–293. https://doi.org/10.1016/0168-1923(95)02265-Y

Oerke, E. C., & Dehne, H. W. (2004). Safeguarding production - Losses in major crops and the role of crop protection. *Crop Protection*, *23*(4), 275–285. https://doi.org/10.1016/j.cropro.2003.10.001

Pan, L., Xia, H., Zhao, X., Guo, Y., & Qin, Y. (2021). Mapping winter crops using a phenology algorithm, time-series sentinel-2 and landsat-7/8 images, and google earth engine. *Remote Sensing*, *13*(13), 1–21. https://doi.org/10.3390/rs13132510

Pastorello, G., Trotta, C., Canfora, E., Chu, H., Christianson, D., Cheah, Y. W., Poindexter, C., Chen, J., Elbashandy, A., Humphrey, M., Isaac, P., Polidori, D., Ribeca, A., van Ingen, C., Zhang, L., Amiro, B., Ammann, C., Arain, M. A., Ardö, J., … Papale, D. (2020). The FLUXNET2015 dataset and the ONEFlux processing pipeline for eddy covariance data. *Scientific Data*, *7*(1). https://doi.org/10.1038/s41597-020-0534-3

Penuelas, J., Filella, I., Biel, C., Serrano, L., & Savé, R. (1993). Penualas 1993.pdf. In *International Journal of Remote Sensing* (Vol. 10, Issue 10, pp. 1887–1905).

Perez-Priego, O. (2021). Plant Chamber Measurements. In *Springer Handbooks*. https://doi.org/10.1007/978-3-030-52171-4_59

Postel, S. L. (2000). *Entering an Era of Water Scarcity : The Challenges Ahead Author (s): Sandra L . Postel Published by : Wiley on behalf of the Ecological Society of America Stable URL : https://www.jstor.org/stable/2641009 Ecological Society of America and Wiley are coll*. *10*(4), 941–948.

Praticò, S., Solano, F., Di Fazio, S., & Modica, G. (2021). Machine learning classification of mediterranean forest habitats in google earth engine based on seasonal sentinel-2 time-series and input image composition optimisation. *Remote Sensing*, *13*(4), 1–28. https://doi.org/10.3390/rs13040586

Purdy, A. J., Fisher, J. B., Goulden, M. L., Colliander, A., Halverson, G., Tu, K., & Famiglietti, J. S. (2018). SMAP soil moisture improves global evapotranspiration. *Remote Sensing of Environment*, *219*(October), 1–14. https://doi.org/10.1016/j.rse.2018.09.023

Reed, B. C., Brown, J. F., VanderZee, D., Loveland, T. R., Merchant, J. W., & Ohlen, D. O. (1994). Measuring phenological variability from satellite imagery. *Journal of Vegetation Science*, *5*(5), 703–714. https://doi.org/10.2307/3235884

Reiche, J. (2015). *Combining SAR and optical satellite image time series for tropical forest monitoring*.

Rosegrant, M. W., Ringler, C., & Zhu, T. (2009). Water for agriculture: Maintaining food security under growing scarcity. *Annual Review of Environment and Resources*, *34*, 205–222. https://doi.org/10.1146/annurev.environ.030308.090351

Schlesinger, W. H., & Jasechko, S. (2014). Transpiration in the global water cycle. *Agricultural and Forest Meteorology*, *189*, 115–117. https://doi.org/10.1016/j.agrformet.2014.01.011

Schlund, M., & Erasmi, S. (2020a). Sentinel-1 time series data for monitoring the phenology of winter wheat. *Remote Sensing of Environment*, *246*. https://doi.org/10.1016/j.rse.2020.111814

Schlund, M., & Erasmi, S. (2020b). Sentinel-1 time series data for monitoring the phenology of winter wheat. *Remote Sensing of Environment*, *246*. https://doi.org/10.1016/j.rse.2020.111814

Schlund, M., & Erasmi, S. (2020c). Sentinel-1 time series data for monitoring the phenology of winter wheat. *Remote Sensing of Environment*, *246*(March), 111814.

https://doi.org/10.1016/j.rse.2020.111814
Seifert Schmidt, C. D., De Carvalho Pereira, F., De Oliveira, A. S., Gomes Júnior, J. F., & Vellame, L. M. (2013). Design , installation and calibration of a weighing lysimeter for crop evapotranspiration studies para estudos de evapotranspiração de culturas agrícolas. *Water Resources and Irrigation Management*, *2*(2), 77–85. https://agris.fao.org/agris-search/search.do?recordID=BR2015301772
Sheikholeslami, S., & Dowling, J. (2019). Ablation Programming for Machine Learning. *Trita-Eecs-Ex*, *Independen*(2019:557), 52. http://urn.kb.se/resolve?urn=urn:nbn:se:kth:diva-258413
SIMS, D. A., & PEARCY, R. W. (1994). Scaling sun and shade photosynthetic acclimation of Alocasia macrorrhiza to whole-plant performance – I. Carbon balance and allocation at different daily photon flux densities. *Plant, Cell & Environment*, *17*(8), 881–887. https://doi.org/10.1111/J.1365-3040.1994.TB00317.X
Sun, H., Xu, A., Lin, H., Zhang, L., & Mei, Y. (2012). Winter wheat mapping using temporal signatures of MODIS vegetation index data. *International Journal of Remote Sensing*, *33*(16), 5026–5042. https://doi.org/10.1080/01431161.2012.657366
Tasumi, M. (2019). Estimating evapotranspiration using METRIC model and Landsat data for better understandings of regional hydrology in the western Urmia Lake Basin. *Agricultural Water Management*, *226*, 105805. https://doi.org/10.1016/J.AGWAT.2019.105805
Torres, R., Snoeij, P., Geudtner, D., Bibby, D., Davidson, M., Attema, E., Potin, P., Rommen, B. Ö., Floury, N., Brown, M., Traver, I. N., Deghaye, P., Duesmann, B., Rosich, B., Miranda, N., Bruno, C., L'Abbate, M., Croci, R., Pietropaolo, A., … Rostan, F. (2012). GMES Sentinel-1 mission. *Remote Sensing of Environment*, *120*, 9–24. https://doi.org/10.1016/j.rse.2011.05.028
Touw, W. G., Bayjanov, J. R., Overmars, L., Backus, L., Boekhorst, J., Wels, M., & Sacha van Hijum, A. F. T. (2013). Data mining in the life science swith random forest: A walk in the park or lost in the jungle? *Briefings in Bioinformatics*, *14*(3), 315–326. https://doi.org/10.1093/bib/bbs034
Troch, F. P. De, Troch, P., & Su, Z. (1997). Use of Remote Sensing Data from Airborne and Spaceborne Active Microwave Sensors Towards Hydrological Modeling. *Undefined*, 171–188. https://doi.org/10.1007/978-94-011-5616-5_15
Tucker, C. J. (1979). Red and photographic infrared linear combinations for monitoring vegetation. *Remote Sensing of Environment*, *8*(2), 127–150. https://doi.org/10.1016/0034-4257(79)90013-0
Van Dam, J. C., Singh, R., Bessembinder, J. J. E., Leffelaar, P. A., Bastiaanssen, W. G. M., Jhorar, R. K., Kroes, J. G., & Droogers, P. (2006). Assessing Options to Increase Water Productivity in Irrigated River Basins Using Remote Sensing and Modelling Tools. *Http://Dx.Doi.Org/10.1080/07900620500405734*, *22*(1), 115–133. https://doi.org/10.1080/07900620500405734
Vanino, S., Nino, P., De Michele, C., Falanga Bolognesi, S., D'Urso, G., Di Bene, C., Pennelli, B., Vuolo, F., Farina, R., Pulighe, G., & Napoli, R. (2018). Capability of Sentinel-2 data for estimating maximum evapotranspiration and irrigation requirements for tomato crop in Central Italy. *Remote Sensing of Environment*, *215*(June), 452–470. https://doi.org/10.1016/j.rse.2018.06.035
Vreugdenhil, M., Wagner, W., Bauer-Marschallinger, B., Pfeil, I., Teubner, I., Rüdiger, C., & Strauss, P. (2018). Sensitivity of Sentinel-1 backscatter to vegetation dynamics: An Austrian case study. *Remote Sensing*, *10*(9), 1–19. https://doi.org/10.3390/rs10091396
Wanniarachchi, S., & Sarukkalige, R. (2022). A Review on Evapotranspiration Estimation in Agricultural Water Management: Past, Present, and Future. *Hydrology*, *9*(7), 1–12. https://doi.org/10.3390/hydrology9070123
Xun, L., Zhang, J., Cao, D., Yang, S., & Yao, F. (2021). A novel cotton mapping index combining Sentinel-1 SAR and Sentinel-2 multispectral imagery. *ISPRS Journal of Photogrammetry and Remote Sensing*, *181*(August), 148–166. https://doi.org/10.1016/j.isprsjprs.2021.08.021
Yang, Y., Anderson, M. C., Gao, F., Wardlow, B., Hain, C. R., Otkin, J. A., Alfieri, J., Yang, Y., Sun, L., &

Dulaney, W. (2018). Field-scale mapping of evaporative stress indicators of crop yield: An application over Mead, NE, USA. *Remote Sensing of Environment*, *210*(March), 387–402. https://doi.org/10.1016/j.rse.2018.02.020

Yao, Y., Liang, S., Cao, B., Liu, S., Yu, G., Jia, K., Zhang, X., Zhang, Y., Chen, J., & Fisher, J. B. (2018a). Satellite Detection of Water Stress Effects on Terrestrial Latent Heat Flux With MODIS Shortwave Infrared Reflectance Data. *Journal of Geophysical Research: Atmospheres*, *123*(20), 11,410-11,430. https://doi.org/10.1029/2018JD029011

Yao, Y., Liang, S., Cao, B., Liu, S., Yu, G., Jia, K., Zhang, X., Zhang, Y., Chen, J., & Fisher, J. B. (2018b). Satellite Detection of Water Stress Effects on Terrestrial Latent Heat Flux With MODIS Shortwave Infrared Reflectance Data. *Journal of Geophysical Research: Atmospheres*, *123*(20), 11,410-11,430. https://doi.org/10.1029/2018JD029011

Zhang, K., Kimball, J. S., & Running, S. W. (2016). A review of remote sensing based actual evapotranspiration estimation. *Wiley Interdisciplinary Reviews: Water*, *3*(6), 834–853. https://doi.org/10.1002/wat2.1168

Zhang, L., Marshall, M., Nelson, A., & Vrieling, A. (2021). A global assessment of PT-JPL soil evaporation in agroecosystems with optical, thermal, and microwave satellite data. *Agricultural and Forest Meteorology*, *306*(May). https://doi.org/10.1016/j.agrformet.2021.108455

Zhen, Z., Chen, S., Yin, T., Chavanon, E., Lauret, N., Guilleux, J., Henke, M., Qin, W., Cao, L., Li, J., Lu, P., & Gastellu-etchegorry, J. P. (2021). Using the negative soil adjustment factor of soil adjusted vegetation index (Savi) to resist saturation effects and estimate leaf area index (lai) in dense vegetation areas. *Sensors*, *21*(6), 1–15. https://doi.org/10.3390/s21062115

(United Nations). (2015). *Facing the challenges : case studies and indicators : UNESCO's contribution to the United Nations world water development report 2015*.

Alam, M. J., Rahman, K. M., Asna, S. M., Muazzam, N., Ahmed, I., & Chowdhury, M. Z. (1996). Comparative studies on IFAT, ELISA & DAT for serodiagnosis of visceral leishmaniasis in Bangladesh. *Bangladesh Medical Research Council Bulletin*, *22*(1), 27–32.

Anderson, M. C., Allen, R. G., Morse, A., & Kustas, W. P. (2012). Use of Landsat thermal imagery in monitoring evapotranspiration and managing water resources. *Remote Sensing of Environment*, *122*, 50–65. https://doi.org/10.1016/j.rse.2011.08.025

Badgley, G., Fisher, J. B., Jiménez, C., Tu, K. P., & Vinukollu, R. (2015). On uncertainty in global terrestrial evapotranspiration estimates from choice of input forcing datasets. *Journal of Hydrometeorology*, *16*(4), 1449–1455. https://doi.org/10.1175/JHM-D-14-0040.1

Becker, F., & Choudhury, B. J. (1988). Relative sensitivity of normalized difference vegetation Index (NDVI) and microwave polarization difference Index (MPDI) for vegetation and desertification monitoring. *Remote Sensing of Environment*, *24*(2), 297–311. https://doi.org/10.1016/0034-4257(88)90031-4

Belgiu, M., & Dra, L. (2016). *ISPRS Journal of Photogrammetry and Remote Sensing Random forest in remote sensing : A review of applications and future directions ˇ gut*. *114*, 24–31. https://doi.org/10.1016/j.isprsjprs.2016.01.011

Belgiu, M., & Drăgu, L. (2016). Random forest in remote sensing: A review of applications and future directions. *ISPRS Journal of Photogrammetry and Remote Sensing*, *114*, 24–31. https://doi.org/10.1016/j.isprsjprs.2016.01.011

Biggs, T. W., Petropoulos, G. P., Velpuri, N. M., Marshall, M., Glenn, E. P., Nagler, P., & Messina, A. (2015). Remote sensing of actual evapotranspiration from croplands. *Remote Sensing of Water Resources, Disasters, and Urban Studies*, *3*, 59–99. https://doi.org/10.1201/b19321

Breiman, L. (2001). *Random Forests*. *45*, 5–32.

Cammalleri, C., Anderson, M. C., Gao, F., Hain, C. R., & Kustas, W. P. (2014). Mapping

daily evapotranspiration at field scales over rainfed and irrigated agricultural areas using remote sensing data fusion. *Agricultural and Forest Meteorology*, *186*, 1–11. https://doi.org/10.1016/j.agrformet.2013.11.001

Chapin, S., Matson, P., & Harold. (2006). *Principles of Terrestrial Ecosystem Ecology - F Stuart Chapin III, Pamela A. Matson, Harold A. Mooney - Google Books*. https://books.google.nl/books?id=shsBCAAAQBAJ&printsec=frontcover&source=gbs_ge_summary_r&cad=0#v=onepage&q&f=false

Chen, J., Jönsson, P., Tamura, M., Gu, Z., Matsushita, B., & Eklundh, L. (2004). A simple method for reconstructing a high-quality NDVI time-series data set based on the Savitzky-Golay filter. *Remote Sensing of Environment*, *91*(3–4), 332–344. https://doi.org/10.1016/j.rse.2004.03.014

Cleugh, H. A., Leuning, R., Mu, Q., & Running, S. W. (2007). Regional evaporation estimates from flux tower and MODIS satellite data. *Remote Sensing of Environment*, *106*(3), 285–304. https://doi.org/10.1016/J.RSE.2006.07.007

Congalton, R. G. (2001). Accuracy assessment and validation of remotely sensed and other spatial information. *International Journal of Wildland Fire*, *10*(3–4), 321–328. https://doi.org/10.1071/wf01031

Darvishzadeh, R., Atzberger, C., Skidmore, A. K., & Abkar, A. A. (2009). Leaf Area Index derivation from hyperspectral vegetation indicesand the red edge position. *International Journal of Remote Sensing*, *30*(23), 6199–6218. https://doi.org/10.1080/01431160902842342

Debats, S. R., Luo, D., Estes, L. D., Fuchs, T. J., & Caylor, K. K. (2016). A generalized computer vision approach to mapping crop fields in heterogeneous agricultural landscapes. *Remote Sensing of Environment*, *179*, 210–221. https://doi.org/10.1016/J.RSE.2016.03.010

Delegido, J., Verrelst, J., Alonso, L., & Moreno, J. (2011). Evaluation of sentinel-2 red-edge bands for empirical estimation of green LAI and chlorophyll content. *Sensors*, *11*(7), 7063–7081. https://doi.org/10.3390/s110707063

Devries, B., Huang, C., Armston, J., Huang, W., Jones, J. W., & Lang, M. W. (2020). *Hydrologic Remote Sensing Branch*. https://doi.org/10.1016/j.rse.2020.111664

El-Baroudy, I., Elshorbagy, A., Carey, S. K., Giustolisi, O., & Savic, D. (2010). Comparison of three data-driven techniques in modelling the evapotranspiration process. *Journal of Hydroinformatics*, *12*(4), 365–379. https://doi.org/10.2166/hydro.2010.029

El Hachimi, J., El Harti, A., Lhissou, R., Ouzemou, J.-E., Chakouri, M., & Jellouli, A. (2022). Combination of Sentinel-2 Satellite Images and Meteorological Data for Crop Water Requirements Estimation in Intensive Agriculture. *Agriculture*, *12*(8), 1168. https://doi.org/10.3390/agriculture12081168

ESA - Sentinel-2. (n.d.). Retrieved August 17, 2023, from https://www.esa.int/Applications/Observing_the_Earth/Copernicus/Sentinel-2

Evangelides, C., & Nobajas, A. (2020). Red-Edge Normalised Difference Vegetation Index (NDVI705) from Sentinel-2 imagery to assess post-fire regeneration. *Remote Sensing Applications: Society and Environment*, *17*. https://doi.org/10.1016/j.rsase.2019.100283

Falge, E., Baldocchi, D., Olson, R., Anthoni, P., Aubinet, M., Bernhofer, C., Burba, G., Ceulemans, R., Clement, R., Dolman, H., Granier, A., Gross, P., Grünwald, T., Hollinger, D., Jensen, N. O., Katul, G., Keronen, P., Kowalski, A., Lai, C. T., … Wofsy, S. (2001). Gap filling strategies for defensible annual sums of net ecosystem exchange. *Agricultural and Forest Meteorology*, *107*(1), 43–69. https://doi.org/10.1016/S0168-1923(00)00225-2

FAO. (2002). *Deficit Irrigation Practices*. https://www.fao.org/3/y3655e/y3655e03.htm

Farg, E., Arafat, S. M., Abd El-Wahed, M. S., & El-Gindy, A. M. (2012). Estimation of

Evapotranspiration ETc and Crop Coefficient K c of Wheat, in south Nile Delta of Egypt Using integrated FAO-56 approach and remote sensing data. *Egyptian Journal of Remote Sensing and Space Science*, *15*(1), 83–89. https://doi.org/10.1016/j.ejrs.2012.02.001

Fernández-Manso, A., Fernández-Manso, O., & Quintano, C. (2016). SENTINEL-2A red-edge spectral indices suitability for discriminating burn severity. *International Journal of Applied Earth Observation and Geoinformation*, *50*, 170–175. https://doi.org/10.1016/j.jag.2016.03.005

Fisher, J. B., Melton, F., Middleton, E., Hain, C., Anderson, M., Allen, R., McCabe, M. F., Hook, S., Baldocchi, D., Townsend, P. A., Kilic, A., Tu, K., Miralles, D. D., Perret, J., Lagouarde, J. P., Waliser, D., Purdy, A. J., French, A., Schimel, D., … Wood, E. F. (2017). The future of evapotranspiration: Global requirements for ecosystem functioning, carbon and climate feedbacks, agricultural management, and water resources. *Water Resources Research*, *53*(4), 2618–2626. https://doi.org/10.1002/2016WR020175

Fisher, J. B., Tu, K. P., & Baldocchi, D. D. (2008). Global estimates of the land-atmosphere water flux based on monthly AVHRR and ISLSCP-II data, validated at 16 FLUXNET sites. *Remote Sensing of Environment*, *112*(3), 901–919. https://doi.org/10.1016/j.rse.2007.06.025

Frampton, W. J., Dash, J., Watmough, G., & Milton, E. J. (2013). Evaluating the capabilities of Sentinel-2 for quantitative estimation of biophysical variables in vegetation. *ISPRS Journal of Photogrammetry and Remote Sensing*, *82*, 83–92. https://doi.org/10.1016/j.isprsjprs.2013.04.007

Friedman, J. H. (n.d.). *No Tit.צלכן*. https://www.ptonline.com/articles/how-to-get-better-mfi-results

Genuer, R., Poggi, J. M., & Tuleau-Malot, C. (2015). VSURF: An R package for variable selection using random forests. *R Journal*, *7*(2), 19–33. https://doi.org/10.32614/rj-2015-018

Gitelson, A. A., Gritz, Y., & Merzlyak, M. N. (2003). Relationships between leaf chlorophyll content and spectral reflectance and algorithms for non-destructive chlorophyll assessment in higher plant leaves. *Journal of Plant Physiology*, *160*(3), 271–282. https://doi.org/10.1078/0176-1617-00887

Gitelson, A. A., Merzlyak, M. N., & Lichtenthaler, H. K. (1996). Detection of red edge position and chlorophyll content by reflectance measurements near 700 nm. *Journal of Plant Physiology*, *148*(3–4), 501–508. https://doi.org/10.1016/S0176-1617(96)80285-9

Glenn, E. P., Nagler, P. L., & Huete, A. R. (2010). Vegetation Index Methods for Estimating Evapotranspiration by Remote Sensing. *Surveys in Geophysics*, *31*(6), 531–555. https://doi.org/10.1007/S10712-010-9102-2/FIGURES/5

Gorrab, A., Ameline, M., Albergel, C., & Baup, F. (2021). Use of sentinel-1 multi-configuration and multi-temporal series for monitoring parameters of winter wheat. *Remote Sensing*, *13*(4), 1–19. https://doi.org/10.3390/rs13040553

Haboudane, D., Miller, J. R., Tremblay, N., Zarco-Tejada, P. J., & Dextraze, L. (2002). Integrated narrow-band vegetation indices for prediction of crop chlorophyll content for application to precision agriculture. *Remote Sensing of Environment*, *81*(2–3), 416–426. https://doi.org/10.1016/S0034-4257(02)00018-4

Hadadi, F., Moazenzadeh, R., & Mohammadi, B. (2022). Estimation of actual evapotranspiration: A novel hybrid method based on remote sensing and artificial intelligence. *Journal of Hydrology*, *609*, 127774. https://doi.org/10.1016/j.jhydrol.2022.127774

Hamrell, M. R. (2014). What is an IND? *FDA Regulatory Affairs: Third Edition*, *266*(April

1995), 41–76. https://doi.org/10.3109/9781420073553-3
Harfenmeister, K., Spengler, D., & Weltzien, C. (2019). Analyzing temporal and spatial characteristics of crop parameters using Sentinel-1 backscatter data. *Remote Sensing*, *11*(13), 1–30. https://doi.org/10.3390/rs11131569
Hatfield, J. L., & Dold, C. (2019). Water-use efficiency: Advances and challenges in a changing climate. *Frontiers in Plant Science*, *10*(February), 1–14. https://doi.org/10.3389/fpls.2019.00103
Hu, X., Shi, L., Lin, G., & Lin, L. (2021a). Comparison of physical-based, data-driven and hybrid modeling approaches for evapotranspiration estimation. *Journal of Hydrology*, *601*, 126592. https://doi.org/10.1016/j.jhydrol.2021.126592
Hu, X., Shi, L., Lin, G., & Lin, L. (2021b). Comparison of physical-based, data-driven and hybrid modeling approaches for evapotranspiration estimation. *Journal of Hydrology*, *601*, 126592. https://doi.org/10.1016/J.JHYDROL.2021.126592
Hu, Y., Buttar, N. A., Tanny, J., Snyder, R. L., Savage, M. J., & Lakhiar, I. A. (2018). Surface Renewal Application for Estimating Evapotranspiration: A Review. *Advances in Meteorology*, *2018*. https://doi.org/10.1155/2018/1690714
Ito, A., Nishina, K., Christopher, P., Reyer, O., Orth, R., Seneviratne, S. I., Rosenzweig, C., Arnell, N. W., Wartenburger, R., Seneviratne, S. I., Hirschi, M., Chang, J., & Ciais, P. (2018). Evapotranspiration simulations in ISIMIP2a — Evaluation of spatio-temporal characteristics with a comprehensive ensemble of independent datasets. *Environmental Research Letters*.
Jiménez, C., Prigent, C., Mueller, B., Seneviratne, S. I., McCabe, M. F., Wood, E. F., Rossow, W. B., Balsamo, G., Betts, A. K., Dirmeyer, P. A., Fisher, J. B., Jung, M., Kanamitsu, M., Reichle, R. H., Reichstein, M., Rodell, M., Sheffield, J., Tu, K., & Wang, K. (2011). Global intercomparison of 12 land surface heat flux estimates. *Journal of Geophysical Research Atmospheres*, *116*(2). https://doi.org/10.1029/2010JD014545
Khalilzadeh, J., & Tasci, A. D. A. (2017). Large sample size, significance level, and the effect size: Solutions to perils of using big data for academic research. *Tourism Management*, *62*, 89–96. https://doi.org/10.1016/j.tourman.2017.03.026
Khan, M. R., de Bie, C. A. J. M., van Keulen, H., Smaling, E. M. A., & Real, R. (2010). Disaggregating and mapping crop statistics using hypertemporal remote sensing. *International Journal of Applied Earth Observation and Geoinformation*, *12*(1), 36–46. https://doi.org/10.1016/j.jag.2009.09.010
Kingston, D. G., Todd, M. C., Taylor, R. G., Thompson, J. R., Arnell, N. W., Kingston, D. G., Todd, M. C., Taylor, R. G., Thompson, J. R., & Arnell, N. W. (2009). Uncertainty in the estimation of potential evapotranspiration under climate change. *Geophysical Research Letters*, *36*(20), 20403. https://doi.org/10.1029/2009GL040267
Kumar, M., Raghuwanshi, N. S., Singh, R., Wallender, W. W., & Pruitt, W. O. (2002). Estimating Evapotranspiration using Artificial Neural Network. *Journal of Irrigation and Drainage Engineering*, *128*(4), 224–233. https://doi.org/10.1061/(ASCE)0733-9437(2002)128:4(224)
Lawrence, R. L., Wood, S. D., & Sheley, R. L. (2006). Mapping invasive plants using hyperspectral imagery and Breiman Cutler classifications (randomForest). *Remote Sensing of Environment*, *100*(3), 356–362. https://doi.org/10.1016/j.rse.2005.10.014
Liou, Y. A., & Kar, S. K. (2014). Evapotranspiration estimation with remote sensing and various surface energy balance algorithms-a review. *Energies*, *7*(5), 2821–2849. https://doi.org/10.3390/en7052821
Liu, Y., Qian, J., & Yue, H. (2021). Comprehensive Evaluation of Sentinel-2 Red Edge and Shortwave-Infrared Bands to Estimate Soil Moisture. *IEEE Journal of Selected Topics in Applied Earth Observations and Remote Sensing*, *14*, 7448–7465.

https://doi.org/10.1109/JSTARS.2021.3098513
Lowder, S. K., Skoet, J., & Raney, T. (2016). The Number, Size, and Distribution of Farms, Smallholder Farms, and Family Farms Worldwide. *World Development*, *87*, 16–29. https://doi.org/10.1016/j.worlddev.2015.10.041
Lu, D., Chen, Q., Wang, G., Liu, L., Li, G., & Moran, E. (2016). A survey of remote sensing-based aboveground biomass estimation methods in forest ecosystems. *International Journal of Digital Earth*, *9*(1), 63–105. https://doi.org/10.1080/17538947.2014.990526
M Bouman, B. A., & J van Kasteren, H. W. (1990). *Ground-Based X-Band (3-cm Wave) Radar Backscattering of Agricultural Crops. II. Wheat, Barley, and Oats; the Impact of Canopy Structure*. *34*, 107–118.
Ma, C., Johansen, K., & McCabe, M. F. (2022). Monitoring Irrigation Events and Crop Dynamics Using Sentinel-1 and Sentinel-2 Time Series. *Remote Sensing*, *14*(5), 1–21. https://doi.org/10.3390/rs14051205
Mandal, D., Kumar, V., Bhattacharya, A., Rao, Y. S., Siqueira, P., & Bera, S. (2018). Sen4Rice: A processing chain for differentiating early and late transplanted rice using time-series sentinel-1 SAR data with google earth engine. *IEEE Geoscience and Remote Sensing Letters*, *15*(12), 1947–1951. https://doi.org/10.1109/LGRS.2018.2865816
Marshall, M., Thenkabail, P., Biggs, T., & Post, K. (2016). Hyperspectral narrowband and multispectral broadband indices for remote sensing of crop evapotranspiration and its components (transpiration and soil evaporation). *Agricultural and Forest Meteorology*, *218–219*, 122–134. https://doi.org/10.1016/j.agrformet.2015.12.025
Marshall, M., Tu, K., & Andreo, V. (2020). On Parameterizing Soil Evaporation in a Direct Remote Sensing Model of ET: PT-JPL. *Water Resources Research*, *56*(5), 1–18. https://doi.org/10.1029/2019WR026290
Maya Gopal, P. S., & Bhargavi, R. (2019). Performance Evaluation of Best Feature Subsets for Crop Yield Prediction Using Machine Learning Algorithms. *Applied Artificial Intelligence*, *33*(7), 621–642. https://doi.org/10.1080/08839514.2019.1592343
Meng, J., Du, X., & Wu, B. (2013). Generation of high spatial and temporal resolution NDVI and its application in crop biomass estimation. *International Journal of Digital Earth*, *6*(3), 203–218. https://doi.org/10.1080/17538947.2011.623189
Moorhead, J. E., Marek, G. W., Gowda, P. H., Lin, X., Colaizzi, P. D., Evett, S. R., & Kutikoff, S. (2019). Evaluation of evapotranspiration from eddy covariance using large weighing lysimeters. *Agronomy*, *9*(2), 1–17. https://doi.org/10.3390/agronomy9020099
Moreira, A., Prats-Iraola, P., Younis, M., Krieger, G., Hajnsek, I., & Papathanassiou, K. P. (2013). A tutorial on synthetic aperture radar. *IEEE Geoscience and Remote Sensing Magazine*, *1*(1), 6–43. https://doi.org/10.1109/MGRS.2013.2248301
Mutanga, O., Adam, E., & Cho, M. A. (2012). High density biomass estimation for wetland vegetation using worldview-2 imagery and random forest regression algorithm. *International Journal of Applied Earth Observation and Geoinformation*, *18*(1), 399–406. https://doi.org/10.1016/j.jag.2012.03.012
Nasirzadehdizaji, R., Sanli, F. B., Abdikan, S., Cakir, Z., Sekertekin, A., & Ustuner, M. (2019). Sensitivity analysis of multi-temporal Sentinel-1 SAR parameters to crop height and canopy coverage. *Applied Sciences (Switzerland)*, *9*(4). https://doi.org/10.3390/app9040655
Nasseri, S., Farhadi Bansouleh, B., & Azari, A. (2023). Estimation of land surface temperature in agricultural lands using Sentinel 2 images: A case study for sunflower fields. *Irrigation and Drainage*, *January*, 796–806. https://doi.org/10.1002/ird.2802
Norman, J. M., Kustas, W. P., & Humes, K. S. (1995). Source approach for estimating soil and vegetation energy fluxes in observations of directional radiometric surface temperature. *Agricultural and Forest Meteorology*, *77*(3–4), 263–293.

https://doi.org/10.1016/0168-1923(95)02265-Y
Oerke, E. C., & Dehne, H. W. (2004). Safeguarding production - Losses in major crops and the role of crop protection. *Crop Protection*, *23*(4), 275–285. https://doi.org/10.1016/j.cropro.2003.10.001
Pan, L., Xia, H., Zhao, X., Guo, Y., & Qin, Y. (2021). Mapping winter crops using a phenology algorithm, time-series sentinel-2 and landsat-7/8 images, and google earth engine. *Remote Sensing*, *13*(13), 1–21. https://doi.org/10.3390/rs13132510
Pastorello, G., Trotta, C., Canfora, E., Chu, H., Christianson, D., Cheah, Y. W., Poindexter, C., Chen, J., Elbashandy, A., Humphrey, M., Isaac, P., Polidori, D., Ribeca, A., van Ingen, C., Zhang, L., Amiro, B., Ammann, C., Arain, M. A., Ardö, J., … Papale, D. (2020). The FLUXNET2015 dataset and the ONEFlux processing pipeline for eddy covariance data. *Scientific Data*, *7*(1). https://doi.org/10.1038/s41597-020-0534-3
Penuelas, J., Filella, I., Biel, C., Serrano, L., & Savé, R. (1993). Penuelas 1993.pdf. In *International Journal of Remote Sensing* (Vol. 10, Issue 10, pp. 1887–1905).
Perez-Priego, O. (2021). Plant Chamber Measurements. In *Springer Handbooks*. https://doi.org/10.1007/978-3-030-52171-4_59
Postel, S. L. (2000). *Entering an Era of Water Scarcity : The Challenges Ahead Author (s): Sandra L . Postel Published by : Wiley on behalf of the Ecological Society of America Stable URL : https://www.jstor.org/stable/2641009 Ecological Society of America and Wiley are coll*. *10*(4), 941–948.
Praticò, S., Solano, F., Di Fazio, S., & Modica, G. (2021). Machine learning classification of mediterranean forest habitats in google earth engine based on seasonal sentinel-2 time-series and input image composition optimisation. *Remote Sensing*, *13*(4), 1–28. https://doi.org/10.3390/rs13040586
Purdy, A. J., Fisher, J. B., Goulden, M. L., Colliander, A., Halverson, G., Tu, K., & Famiglietti, J. S. (2018). SMAP soil moisture improves global evapotranspiration. *Remote Sensing of Environment*, *219*(October), 1–14. https://doi.org/10.1016/j.rse.2018.09.023
Reed, B. C., Brown, J. F., VanderZee, D., Loveland, T. R., Merchant, J. W., & Ohlen, D. O. (1994). Measuring phenological variability from satellite imagery. *Journal of Vegetation Science*, *5*(5), 703–714. https://doi.org/10.2307/3235884
Reiche, J. (2015). *Combining SAR and optical satellite image time series for tropical forest monitoring*.
Rosegrant, M. W., Ringler, C., & Zhu, T. (2009). Water for agriculture: Maintaining food security under growing scarcity. *Annual Review of Environment and Resources*, *34*, 205–222. https://doi.org/10.1146/annurev.environ.030308.090351
Schlesinger, W. H., & Jasechko, S. (2014). Transpiration in the global water cycle. *Agricultural and Forest Meteorology*, *189*, 115–117. https://doi.org/10.1016/j.agrformet.2014.01.011
Schlund, M., & Erasmi, S. (2020a). Sentinel-1 time series data for monitoring the phenology of winter wheat. *Remote Sensing of Environment*, *246*. https://doi.org/10.1016/j.rse.2020.111814
Schlund, M., & Erasmi, S. (2020b). Sentinel-1 time series data for monitoring the phenology of winter wheat. *Remote Sensing of Environment*, *246*. https://doi.org/10.1016/j.rse.2020.111814
Schlund, M., & Erasmi, S. (2020c). Sentinel-1 time series data for monitoring the phenology of winter wheat. *Remote Sensing of Environment*, *246*(March), 111814. https://doi.org/10.1016/j.rse.2020.111814
Seifert Schmidt, C. D., De Carvalho Pereira, F., De Oliveira, A. S., Gomes Júnior, J. F., & Vellame, L. M. (2013). Design , installation and calibration of a weighing lysimeter for

crop evapotranspiration studies para estudos de evapotranspiração de culturas agrícolas. *Water Resources and Irrigation Management*, *2*(2), 77–85. https://agris.fao.org/agris-search/search.do?recordID=BR2015301772

Sheikholeslami, S., & Dowling, J. (2019). Ablation Programming for Machine Learning. *Trita-Eecs-Ex*, *Independen*(2019:557), 52. http://urn.kb.se/resolve?urn=urn:nbn:se:kth:diva-258413

SIMS, D. A., & PEARCY, R. W. (1994). Scaling sun and shade photosynthetic acclimation of Alocasia macrorrhiza to whole-plant performance – I. Carbon balance and allocation at different daily photon flux densities. *Plant, Cell & Environment*, *17*(8), 881–887. https://doi.org/10.1111/J.1365-3040.1994.TB00317.X

Sun, H., Xu, A., Lin, H., Zhang, L., & Mei, Y. (2012). Winter wheat mapping using temporal signatures of MODIS vegetation index data. *International Journal of Remote Sensing*, *33*(16), 5026–5042. https://doi.org/10.1080/01431161.2012.657366

Tasumi, M. (2019). Estimating evapotranspiration using METRIC model and Landsat data for better understandings of regional hydrology in the western Urmia Lake Basin. *Agricultural Water Management*, *226*, 105805. https://doi.org/10.1016/J.AGWAT.2019.105805

Torres, R., Snoeij, P., Geudtner, D., Bibby, D., Davidson, M., Attema, E., Potin, P., Rommen, B. Ö., Floury, N., Brown, M., Traver, I. N., Deghaye, P., Duesmann, B., Rosich, B., Miranda, N., Bruno, C., L'Abbate, M., Croci, R., Pietropaolo, A., … Rostan, F. (2012). GMES Sentinel-1 mission. *Remote Sensing of Environment*, *120*, 9–24. https://doi.org/10.1016/j.rse.2011.05.028

Touw, W. G., Bayjanov, J. R., Overmars, L., Backus, L., Boekhorst, J., Wels, M., & Sacha van Hijum, A. F. T. (2013). Data mining in the life science swith random forest: A walk in the park or lost in the jungle? *Briefings in Bioinformatics*, *14*(3), 315–326. https://doi.org/10.1093/bib/bbs034

Troch, F. P. De, Troch, P., & Su, Z. (1997). Use of Remote Sensing Data from Airborne and Spaceborne Active Microwave Sensors Towards Hydrological Modeling. *Undefined*, 171–188. https://doi.org/10.1007/978-94-011-5616-5_15

Tucker, C. J. (1979). Red and photographic infrared linear combinations for monitoring vegetation. *Remote Sensing of Environment*, *8*(2), 127–150. https://doi.org/10.1016/0034-4257(79)90013-0

Van Dam, J. C., Singh, R., Bessembinder, J. J. E., Leffelaar, P. A., Bastiaanssen, W. G. M., Jhorar, R. K., Kroes, J. G., & Droogers, P. (2006). Assessing Options to Increase Water Productivity in Irrigated River Basins Using Remote Sensing and Modelling Tools. *Http://Dx.Doi.Org/10.1080/07900620500405734*, *22*(1), 115–133. https://doi.org/10.1080/07900620500405734

Vanino, S., Nino, P., De Michele, C., Falanga Bolognesi, S., D'Urso, G., Di Bene, C., Pennelli, B., Vuolo, F., Farina, R., Pulighe, G., & Napoli, R. (2018). Capability of Sentinel-2 data for estimating maximum evapotranspiration and irrigation requirements for tomato crop in Central Italy. *Remote Sensing of Environment*, *215*(June), 452–470. https://doi.org/10.1016/j.rse.2018.06.035

Vreugdenhil, M., Wagner, W., Bauer-Marschallinger, B., Pfeil, I., Teubner, I., Rüdiger, C., & Strauss, P. (2018). Sensitivity of Sentinel-1 backscatter to vegetation dynamics: An Austrian case study. *Remote Sensing*, *10*(9), 1–19. https://doi.org/10.3390/rs10091396

Wanniarachchi, S., & Sarukkalige, R. (2022). A Review on Evapotranspiration Estimation in Agricultural Water Management: Past, Present, and Future. *Hydrology*, *9*(7), 1–12. https://doi.org/10.3390/hydrology9070123

Xun, L., Zhang, J., Cao, D., Yang, S., & Yao, F. (2021). A novel cotton mapping index combining Sentinel-1 SAR and Sentinel-2 multispectral imagery. *ISPRS Journal of*

Photogrammetry and Remote Sensing, *181*(August), 148–166. https://doi.org/10.1016/j.isprsjprs.2021.08.021

Yang, Y., Anderson, M. C., Gao, F., Wardlow, B., Hain, C. R., Otkin, J. A., Alfieri, J., Yang, Y., Sun, L., & Dulaney, W. (2018). Field-scale mapping of evaporative stress indicators of crop yield: An application over Mead, NE, USA. *Remote Sensing of Environment*, *210*(March), 387–402. https://doi.org/10.1016/j.rse.2018.02.020

Yao, Y., Liang, S., Cao, B., Liu, S., Yu, G., Jia, K., Zhang, X., Zhang, Y., Chen, J., & Fisher, J. B. (2018a). Satellite Detection of Water Stress Effects on Terrestrial Latent Heat Flux With MODIS Shortwave Infrared Reflectance Data. *Journal of Geophysical Research: Atmospheres*, *123*(20), 11,410-11,430. https://doi.org/10.1029/2018JD029011

Yao, Y., Liang, S., Cao, B., Liu, S., Yu, G., Jia, K., Zhang, X., Zhang, Y., Chen, J., & Fisher, J. B. (2018b). Satellite Detection of Water Stress Effects on Terrestrial Latent Heat Flux With MODIS Shortwave Infrared Reflectance Data. *Journal of Geophysical Research: Atmospheres*, *123*(20), 11,410-11,430. https://doi.org/10.1029/2018JD029011

Zhang, K., Kimball, J. S., & Running, S. W. (2016). A review of remote sensing based actual evapotranspiration estimation. *Wiley Interdisciplinary Reviews: Water*, *3*(6), 834–853. https://doi.org/10.1002/wat2.1168

Zhang, L., Marshall, M., Nelson, A., & Vrieling, A. (2021). A global assessment of PT-JPL soil evaporation in agroecosystems with optical, thermal, and microwave satellite data. *Agricultural and Forest Meteorology*, *306*(May). https://doi.org/10.1016/j.agrformet.2021.108455

Zhen, Z., Chen, S., Yin, T., Chavanon, E., Lauret, N., Guilleux, J., Henke, M., Qin, W., Cao, L., Li, J., Lu, P., & Gastellu-etchegorry, J. P. (2021). Using the negative soil adjustment factor of soil adjusted vegetation index (Savi) to resist saturation effects and estimate leaf area index (lai) in dense vegetation areas. *Sensors*, *21*(6), 1–15. https://doi.org/10.3390/s21062115

7.0 APPENDICES

Appendix 1. scatter plot for scenario 4 (Rainfed)

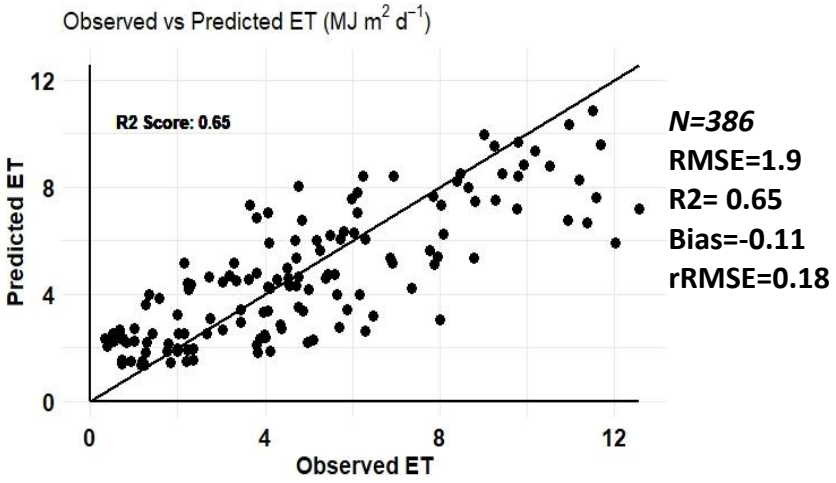

Appendix 2. Scatter plot for scenario 5 (Rainfed, S-2 only)

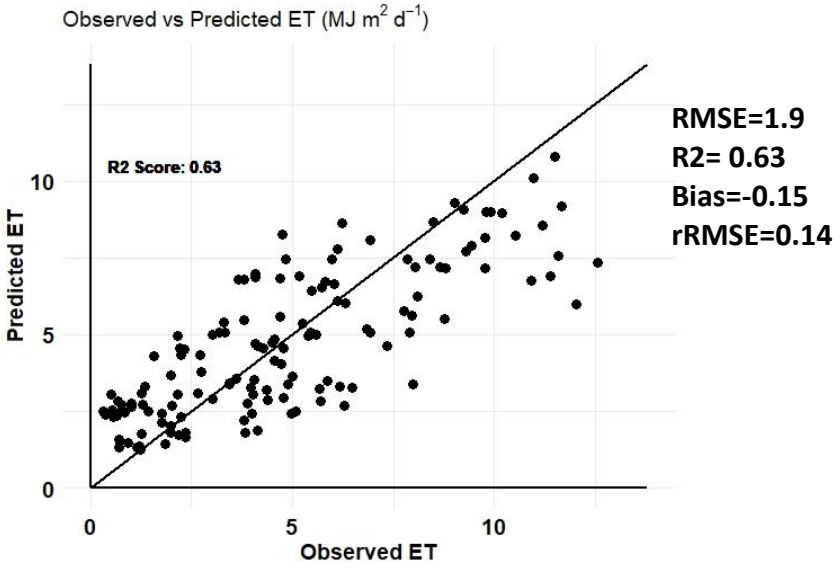

Appendix 3. Scatter plot for scenario 6 (Rainfed, S-1 only)

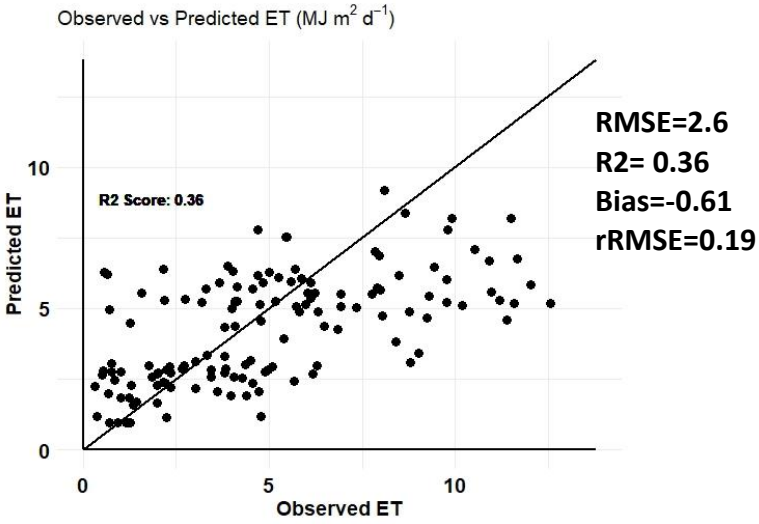

Appendix 4. Scatterplot for scenario 7 (Irrigated, all sensors).

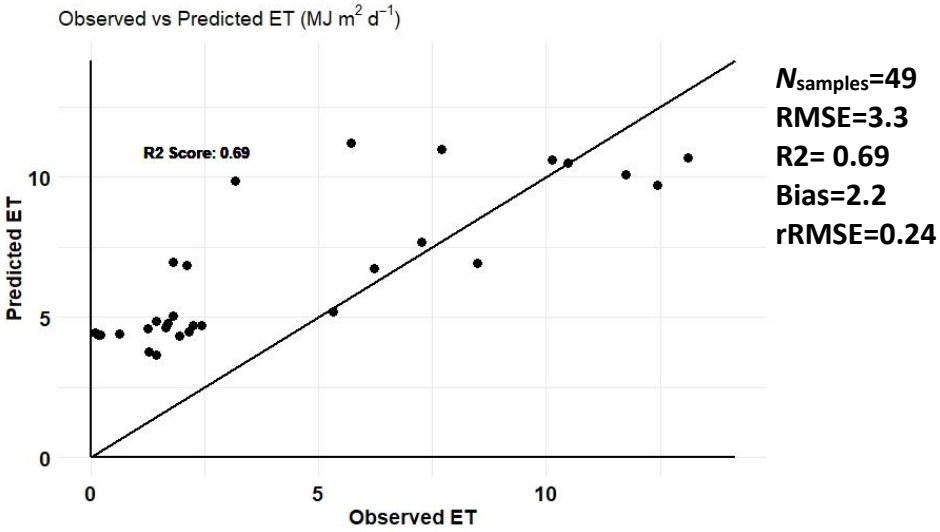

Appendix 5. scatterplot for scenario 8 (Irrigated ,S-2 Only).

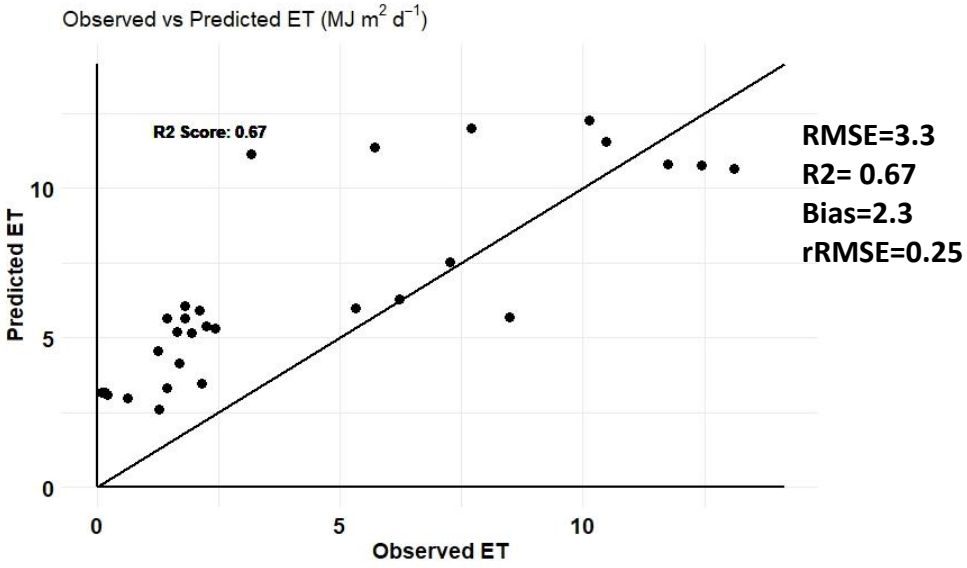

Appendix 6. Scatterplot for scenario 9 (Irrigated S-1 Only).